

CHAPTER 2

2. Results and Discussion

2.1. Design strategy

As described in the BTK inhibitors section, most of the advanced BTK inhibitors are covalent. Covalent inhibition of kinases by targeting a non-catalytic cysteine residue is a validated strategy for achieving sustained target engagement without requiring high systemic drug exposure [116, 117]. In the BTK enzyme structure, Cys481 is proximal to the ATP binding site, and that analogous cysteine residue is present in a few other human kinases. The relatively low prevalence of the corresponding cysteine residue in the human kinome makes covalent inhibition of BTK an attractive strategy for achieving high selectivity [118].

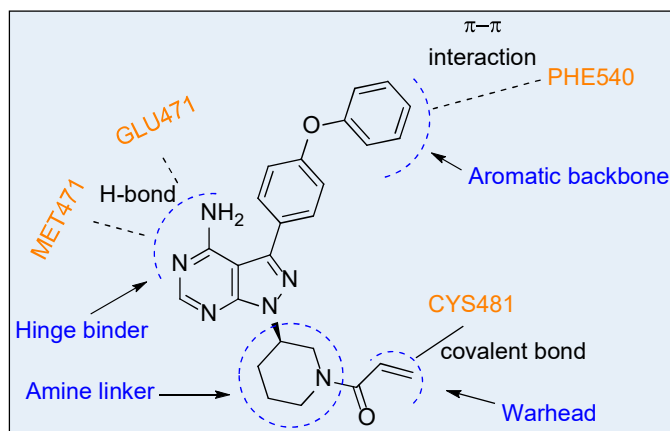


Figure 10. Common binding interactions and features of the BTK inhibitor (Ibrutinib)

Based on the co-crystal structure of IBR with BTK enzyme, IBR structure can be categorized into four parts: Hinge binder, Amine linker, Aromatic backbone, and Warhead (**Figure 10**) [119]. The hinge binder (pyrazolo [3,4-d]pyrimidin-4-amine) forms hydrogen bonding with the Met477 (at hinge region) and Glu475, in the active site of BTK. These interactions are very crucial for the BTK inhibitory activity. While

piperidine amine acts as a linker and provides spatial angle so that warhead (acrylamide moiety) can interact covalently with Cys481 [119].

Aromatic backbone (biphenyl ether) orients towards the back side pocket of Thr474 and exhibit π - π stacking interactions with the Phe540 of a BTK enzyme. The crucial hinge binder pyrazolo[3,4-d]pyrimidin-4-amine core was considered as a starting point. In the present investigation, stepwise structural modifications were carried out in the IBR to discover novel, potent, selective and orally bioavailable BTK inhibitor. Initially, to improve BTK enzyme selectivity, while retaining potency, a series of compounds (**24a-h**) were designed to identify the novel amine linker. Subsequently, to optimise the aromatic backbone, warhead moiety, and central core, the second (**32a-an**), third (**32ao-av**), and fourth (**41**, **42**, **51**, **52**, **61**, **62**, **71**, and **72**) series of compounds were designed (Figure 11).

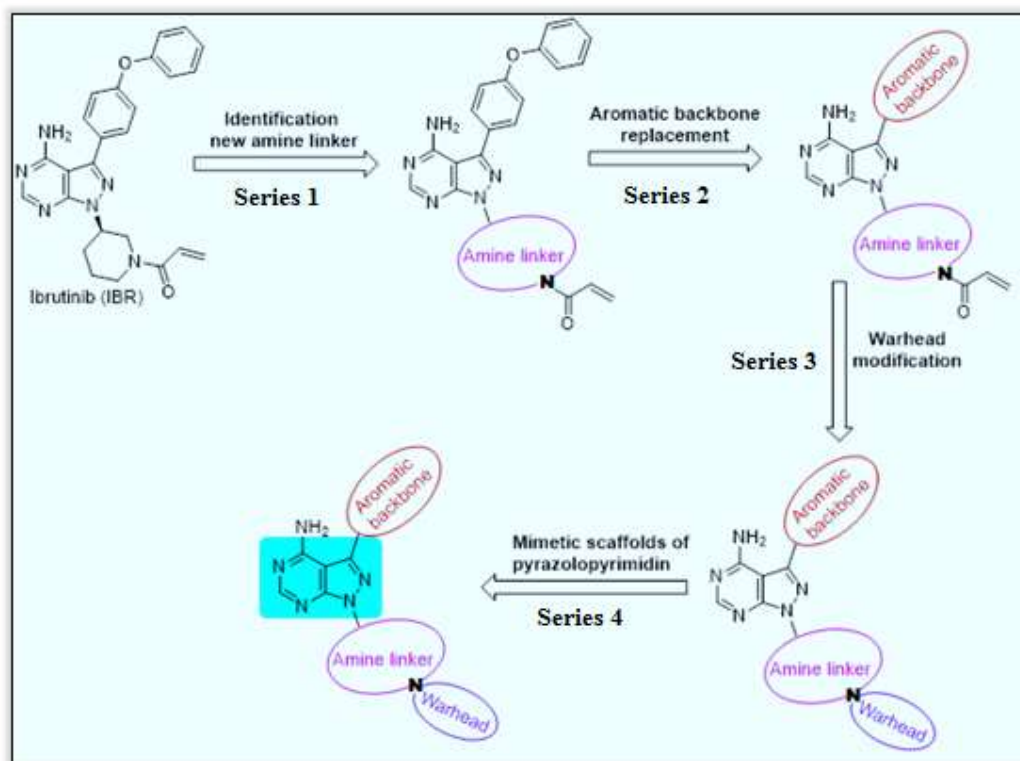


Figure 11. Methodology for designing novel BTK inhibitors

The amine linker is an integral part of BTK inhibitors that provide spatial orientation to the warhead. As per the findings, the piperidine or pyrrolidine ring functions as amine linkers in most of the known BTK inhibitors. According to preliminary molecular modelling results, there is enough space in the ATP binding site of BTK to accommodate a saturated bicyclic ring system. Hence, in **Series 1**, we have selected some saturated bicyclic amines as linkers for bioisosteric replacement of piperidine in IBR and synthesised a total of eight target compounds (**24a-h**) by employing **Scheme 4**.

After discovering the amine linker, which has superior biological potency in **Series 1**, we will make subsequent efforts to optimise the aromatic backbone component of the BTK inhibitor in **Series 2**. According to a molecular modelling analysis, the aromatic backbone adopts a favourable orientation in the hydrophobic pocket of the BTK enzyme, enabling it to interact with the vital residues (Thr474 and Phe540) of the hydrophobic pocket. The docking study additionally revealed that if a hydrogen bond acceptor is introduced into the aromatic backbone, additional hydrogen bond interactions with Ser538 and/or Lys430 may occur, eventually leading to kinase selectivity [119].

These findings led to the selection of three sets of aromatic backbone bioisosteres in **Series 2**. In the first set of **Series 2**, benzamide and picolinamide derivatives were designed, whereas in the second set of **Series 2**, 4-phenyl ether, 4-phenyl thioether, and 4-phenyl alkyl derivatives were used as the aromatic backbones. Phenyl-containing fused heterocycles were enlisted as the aromatic backbone for the third set of **Series 2**. In accordance with the synthetic route given in **Scheme 6**, forty compounds (**32a-an**) prepared in **Series 2** and screened for *in vitro* activities.

Electrophilic warheads, which feature in the design of BTK inhibitors, interact covalently with the nucleophilic Cys481 of the BTK enzyme. In **Series 3**, to study the influence of warheads on BTK inhibitory activities, selected Michael acceptors and other moiety were utilised as warheads instead of conventional acrylamide. In **Series 3**, a total of eight compounds (**32ao-av**) were synthesised using **Scheme 7**,

Pyrazolo-pyrimidine-4-amine is a key pharmacophore and interacts with the hinge region of BTK enzyme through the hydrogen bonding. It also provides orientation to the aromatic backbone and linker, which create a "Y" shape that is essential for BTK inhibitory activities. In **Series 4**, we intended to incorporate certain mimetic heterocycles of Pyrazolo-pyrimidine, such as Pyrrolo-pyrimidin, Oxo-purine, Imidazo-pyrazine, and Pyrazole scaffolds, in place of Pyrazolo-pyrimidine. In **Series 4**, eight compounds (**41, 42, 51, 52, 61, 62, 71, and 72**) were synthesised following the synthetic method described in **Schemes 8, 9, 10, and 11**.

Finally, the most promising compound out of the four series (64 target compounds) was evaluated for *in vivo* pharmacological studies.

2.2. 3-(4-phenoxyphenyl)-pyrazolo[3,4-d]pyrimidin-4-amine scaffold based BTK inhibitors 24a-h (Series 1)

2.2.1. Chemistry

In our initial investigation, we selected eight saturated bicyclic amine rings for bioisosteric replacement of piperidine in IBR and synthesised eight target compounds (**24a-h**) in the **Series 1** as novel BTK inhibitors (**Figure 12**).

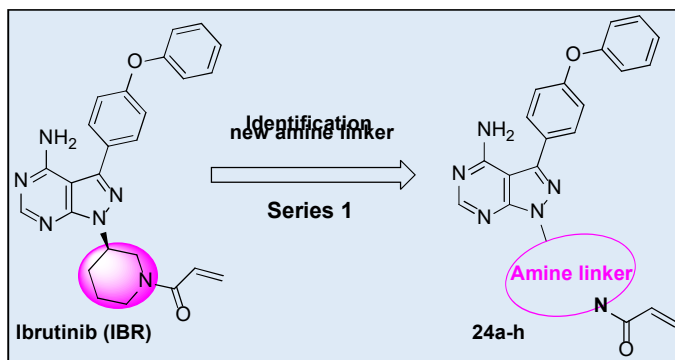
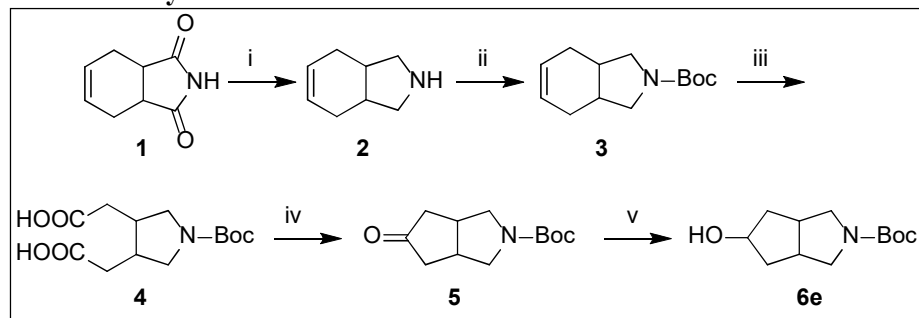


Figure 12. Designing of 3-(4-phenoxyphenyl)-pyrazolo[3,4-d] pyrimidin-4-amine scaffold-based BTK inhibitors 24a-h of Series 1

The target compounds (**24a–h**) of **Series 1** were synthesised by modifying the literature procedure, as shown in **Scheme 4**. The key intermediates **6e**, **6g**, and **6h** are synthesised as depicted in **Schemes 1**, **2**, and **3**, respectively. Intermediates **6a**, **6b**, **6c**, **6d**, and **6f** were obtained from an in-house chemical library, while others were procured from a commercial vendor.

Scheme 1 was adopted to prepare intermediate **6e**, which starts with the reduction of tetrahydrophthalimide. The obtained amine (**2**) was Boc protected with triethyl amine and Boc anhydride, followed by ruthenium oxide catalysed oxidation to yield dicarboxylic acid (**4**). To obtain the keto intermediate (**5**), the intermediate **4** was subjected to a modified Dieckmann reaction. Sodium borohydride was used to reduce the keto intermediate (**5**) to get an alcohol intermediate **6e** (see experimental section 4.1.1. for detailed procedures).

Scheme 1: Synthetic route of intermediate 6e

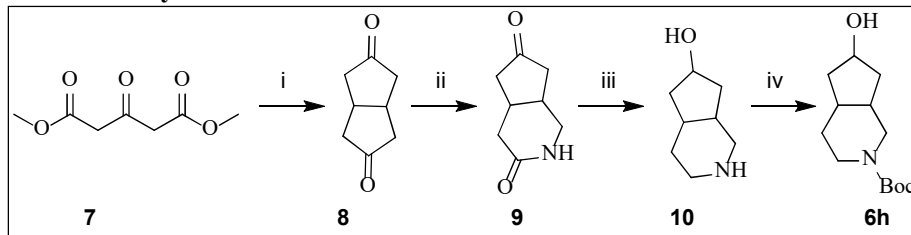


Reagents and conditions: i) Lithium aluminium hydride, THF, 60°C, 18 h, 80%; ii) Boc anhydride, TEA, THF, 25°C, 18 h, 96%; iii) Sodium meta periodate, ruthenium(IV) oxide

hydrate, EtOAc, H₂O, 25°C, 4 h, 78%; iv) Acetic anhydride, sodium acetate anhydrous, 130°C, 1 h, 65%; v) Sodium borohydride, MeOH, 0°C, 2 h, 98%.

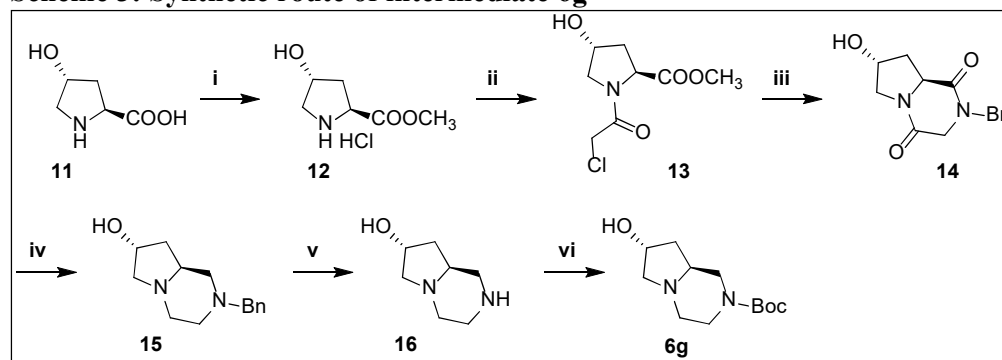
Scheme 2 displays the synthetic pathway for the intermediate **6h**. The first step involved reacting dimethyl 3-oxopentanedioate with glyoxal and sodium hydroxide, which was followed by acidic decarboxylation, which resulted in a diketo intermediate (**8**). Using the Schmidt reaction condition, intermediate **8** was converted to intermediate **9**, and the ketoamide intermediate (**9**) was reacted with lithium aluminium hydride to form an aminoalcohol moiety (**10**), which was Boc protected using Boc anhydride to synthesise intermediate **6h** (see experimental section 4.1.2. for detailed procedures).

Scheme 2: Synthetic route of intermediate 6h



Reagents and conditions: i) Glyoxal, sodium hydroxide, MeOH, 65°C, 2 h, hydrochloric acid, AcOH, reflux, 3 h, 53%; ii) Sodium azide, hydrochloric acid, 25°C, 15 h, 46%; iii) Lithium aluminium hydride, THF, 60°C, 5 h, 95%; iv) Boc anhydride, sodium carbonate, ACN, H₂O, 25°C, 3 h, 92%.

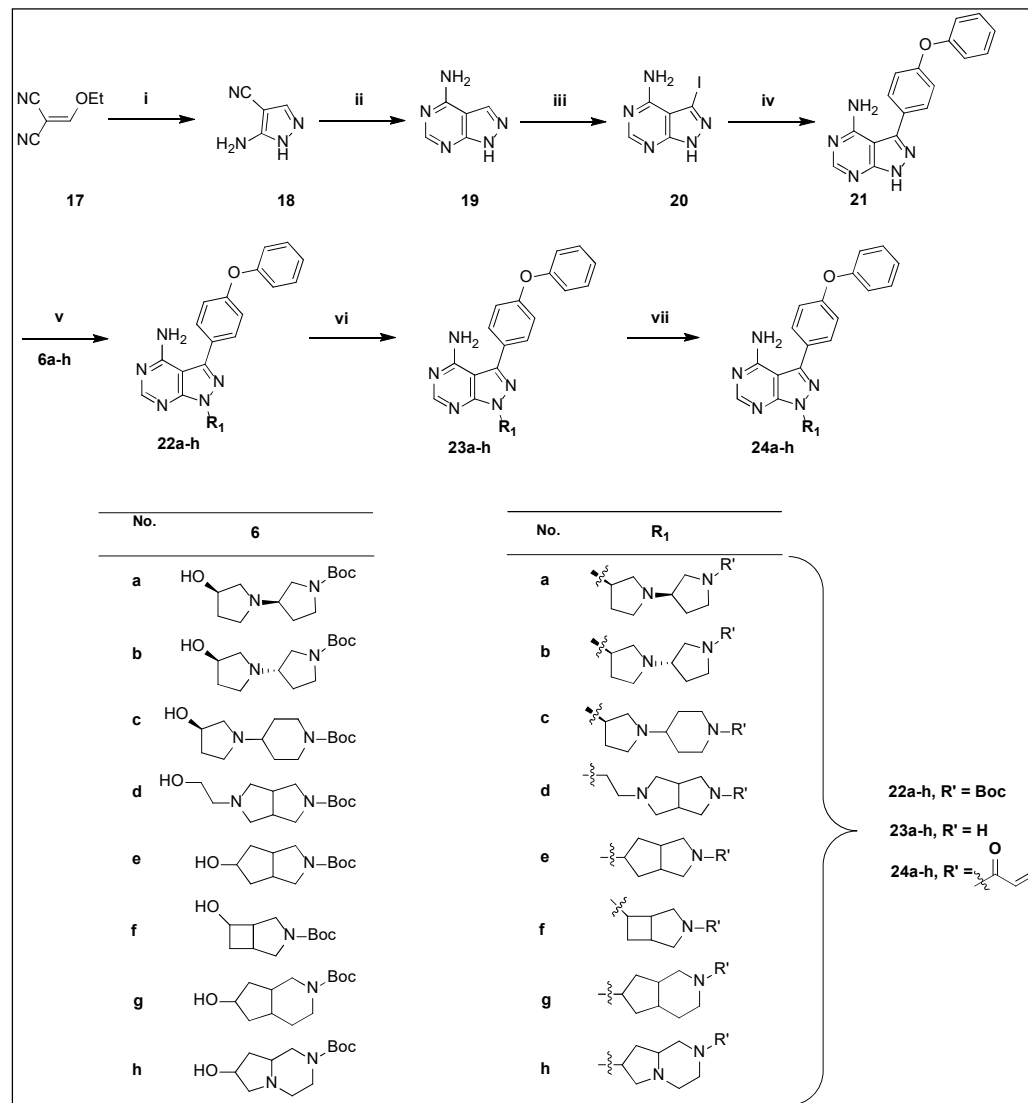
In accordance with **Scheme 3**, Intermediate **6g** was synthesized. The esterification of trans-4-hydroxy-L-proline was done using acetyl chloride and methanol, sequentially coupled with chloroacetyl chloride to get **12**. Intermediate **13** was heated with benzylamine and triethylamine to obtain diamide (**14**), which was then reduced to amine (**15**) by refluxing it with lithium aluminium hydride. Palladium-catalyzed hydrogenation was carried out to debenzylate **16**, followed by Boc protection of **16** to provide the intermediate **6g** (see experimental section 4.1.3. for detailed procedures).

Scheme 3: Synthetic route of intermediate 6g

Reagents and conditions: i) Acetyl chloride, MeOH, 65°C, 5 h, 83%; ii) Chloroacetyl chloride, benzene, 80°C, 18 h, 62%; iii) Benzylamine, triethylamine, 125°C, 20 h, 78%; iv) Lithium aluminium hydride, THF, 80°C, 20 h, 65%; v) Pd/C, H_{2(g)}, MeOH, 25°C, 18 h, 95%; vi) Boc anhydride, sodium carbonate, ACN, H₂O, 25°C, 8 h, 93%.

For the synthesis of target molecules **24a-h** (**Scheme 4**), commercially available (Ethoxymethylene) malononitrile (**17**) reacted with hydrazine hydrate to produce 5-amino-1H-pyrazole-4-carbonitrile (**18**), which was then converted to 1H-pyrazolo[3,4-d]pyrimidin-4-amine (**19**) by reacting with formamide. Intermediate **19** was iodinated with N-iodosuccinimide to yield iodo intermediate **20**, followed by being subjected to a Suzuki-Miyaura coupling reaction with 4-phenoxyphenyl boronic acid to make the 3-(4-phenoxyphenyl)-1H-pyrazolo[3,4-d]pyrimidin-4-amine (**21**). Mitsunobu reactions of intermediate **21** with various substituted alcohols (**6a-h**) in the presence of diisopropyl azodicarboxylate and triphenyl phosphine obtained intermediates (**22a-h**). The tert-butyl carbamate group of **23a-h** was deprotected with trifluoroacetic acid, followed by acylation with acryloyl chloride in the presence of a base to give target compounds (**24a-h**). All of the target compounds were characterized by NMR, ESI-MS, UPLC, and CHN analysis. The experimental section 4.1.4., fully describes the procedures for preparing the target compounds, their yields, and melting points.

Scheme 4: Synthetic route of 24a-h of Series 1



Reagents and conditions: i) Hydrazine hydrate, 110°C, 3 h, 69%; ii) Formamide, 180°C, 5 h, 87%; iii) N-iodosuccinimide, DMF, 80°C, 18 h, 85%; iv) 4-phenoxyphenyl boronic acid, PdCl₂(PPh₃)₂, KHCO₃(aq), DMF, 90°C, 5 h, 74%; v) **6a-h**, diisopropyl azodicarboxylate, triphenyl phosphine, THF, 25°C, 18 h, 43-68%; vi) Trifluoroacetic acid, DCM, 25°C, 3 h, 87-95%; vii) Acryloyl chloride, N,N-Diisopropylethylamine, DCM, 0°C to 25°C, 18 h, 38-63%.

2.2.2. Biological evaluation of Series 1

2.2.2.1. *In vitro* BTK inhibitory and anti-proliferative activity

The synthesised compounds (**24a-h**) were assessed for their *in vitro* BTK inhibitory activity using a cell-free biochemical assay. Briefly, a fixed amount of recombinant purified human BTK (3 ng/reaction) was incubated with increasing concentrations of

test compounds. An enzymatic reaction was initiated by adding a substrate cocktail containing ATP (50 $\mu\text{mol/L}$) to 96-well plates. The reaction was incubated at room temperature for 2 h, followed by quantification of the leftover ATP, according to the manufacturer's protocol, using ADP-Glo reagent. Data were plotted using 'enzyme with no inhibitor' as the 100% kinase (for more information, see experimental section 4.2.1.).

The anti-proliferative activity of test compounds (**24a-h**) were evaluated *in vitro* in the human diffuse large B-cell lymphoma (DLBCL) cell line TMD8. Briefly, defined numbers of TMD8 cells were incubated in 96-well plates with increasing concentrations of test compounds. Cell growth was measured using the MTT assay, and IC_{50} values were determined by nonlinear regression using the Graph Pad Prism 6 software (for detail procedures, see experimental section 4.2.2.). IBR was taken as the positive control, and it showed IC_{50} values of 1.1 nM and 1.2 nM in the BTK enzyme and TMD8 cell proliferation assays, respectively.

Saturated bicyclic amines (**6a-h**) were introduced as amine linker and overall, eight compounds (**24a-h**) were synthesized in this **Series 1**. Test compounds were screened in both the *in vitro* assays (**Table 2**). Except for **24c** and **24f**, all of the test compounds (**24a-h**) had IC_{50} values in the single digits in both assays. The low potency could be attributed to the amine linkers of **24c** and **24f** failing to orient the warhead component towards Cys481 and thus missing the covalent interaction. The octahydrocyclopenta[c]pyrrole analogue (**24e**) was discovered to be the best amine linker among **24a-h**, which had BTK enzyme inhibitory ($\text{IC}_{50} = 1.4$ nM) and anti-proliferative ($\text{IC}_{50} = 0.5$ nM) activity comparable to IBR. While **24b** demonstrated the second-best inhibitory activity, with IC_{50} values of 2.8 nM (BTK enzyme) and 1.4 nM (TMD8 cell proliferation), it clearly shows that a five-membered ring combination was

best suited as an amine linker. Enantiomer **24a** of **24b** was less potent in the BTK enzyme ($IC_{50} = 5.1$ nM) and TMD8 cell proliferation ($IC_{50} = 4.4$ nM) assays than **24b**, which may have been affected by its spatial position. Amine linker with ethyl spacer (**24d**) significantly reduced BTK enzyme inhibitory ($IC_{50} = 8.1$ nM) and anti-proliferative ($IC_{50} = 11$ nM) activities, and ring expansion (six-membered) of amine linker (**24g** and **24h**) had relatively lower BTK enzyme ($IC_{50} = 2.9$ and 3.6 nM) and TMD8 cell proliferation ($IC_{50} = 2.8$ and 3.3 nM) inhibition.

Thus, **24e** demonstrated the best *in vitro* inhibitory activities in **Series 1**, and the fact that it was also comparable to IBR piqued our interest in further investigating it in biological studies such as CYP and hERG inhibitory activities.

Table 2. *In vitro* BTK enzyme and TMD8 cell proliferation inhibitory data of **24a–h** of Series 1

Comp.	R ₁	BTK IC ₅₀ (nM) ^a	TMD8 IC ₅₀ (nM) ^b	Comp.	R ₁	BTK IC ₅₀ (nM) ^a	TMD8 IC ₅₀ (nM) ^b
24a		5.1	4.4	24e		1.4	0.5
24b		2.8	1.4	24f		29	21
24c		38	46	24g		2.9	2.8
24d		8.1	11	24h		3.6	3.3
	IBR	1.1	1.2				

All the data are shown as the mean for three experiments. ^a BTK inhibition (IC_{50}) determination using *in vitro* BTK kinase assay on ADP Glo platform, ^b TMD8 cytotoxicity inhibition (IC_{50}) determination using TMD8 cell lines assay.

2.2.2.2. CYP and hERG inhibitory activities of the lead compound of Series 1

Compound **24e** was incubated with human liver microsomes and NADPH in the presence of CYP-specific substrates to evaluate CYP inhibitory activities (for detail procedures, see experimental section 4.2.3.). The automated patch clamp assay was

used to assess hERG inhibitory activities. At 10 μM concentration (for detail procedures, see experimental section 4.2.4.), it was found to inhibit hERG and CYP (1A2, 2C9, 2D6, 2C19, and 3A4) by less than 50%, as depicted in **Table 3**.

Table 3. CYP and hERG inhibitory activity of the lead compound of Series 1

Comp.	%hERG inhibition ^a @ 10 μM	% CYP inhibition ^b @ 10 μM					
		CYP1A2	CYP2C8	CYP2C9	CYP2D6	CYP2C19	CYP3A4
24e	54	14	16	40	19	9	8
IBR	35	NI	81	86	31	39	55

^a In the automated patch clamp assay, ^b incubated test compound with human liver microsomes and NADPH in the presence of CYP specific substrate, value are mean of three repeat experiment, NI = No inhibition.

2.2.2.3. Pharmacokinetic studies of 24e of Series 1

Compound **24e** demonstrated excellent *in vitro* activity and was found to be devoid of CYP and hERG liabilities. So, it was subjected to an *in vivo* pharmacokinetic study in male BALB/c mice and Wister rats (see experimental section 4.2.5.). In single-dose PK studies (3 mg/kg, po, and 1 mg/kg, iv) of compounds **24e** and IBR, various PK parameters (T_{max} , C_{max} , $T_{1/2}$, CL, AUC, and %F) were recorded (**Table 4**). The PK study in mice and rats reveals that 24e have a slightly better PK profile (C_{max} = 282 and 283 ng/mL, AUC = 433 and 301 ng.h/mL, %F = 36 and 25, in mice and rats, respectively) compared to IBR (**Table 4**).

Table 4. Pharmacokinetic profile^a of 24e

Dose	Parameters	24e		IBR	
		<i>Mice</i>	<i>Rat</i>	<i>Mice</i>	<i>Rat</i>
IV 1 mg kg ⁻¹	AUC (ng.h/mL)	401	370	151	250
	V _{ss} (L/kg)	0.90	1.37	0.50	1.50
	CL (ml/min/kg)	48.1	49.9	27.5	66.3
	$T_{1/2}$ (h)	0.35	0.39	0.20	0.40
PO 3 mg kg ⁻¹	T_{max} (h)	0.25	0.25	0.25	0.25
	C_{max} (ng/mL)	282	283	402	129
	AUC (ng.h/mL)	433	301	277	86
	$T_{1/2}$ (h)	0.56	1.08	0.30	0.80

%F*	36	25	15	11
^a In male BALB/c mice and male Wister rats (n = 3), compounds were administered orally (po) at 3 mg/kg dose and plasma concentration was analyzed by LC-MS, values indicate Mean. *Oral bioavailability (%F) was calculated wrt to iv AUC. Test Compounds were administered at 1 mg/kg dose.				

2.2.3. Molecular docking study of 24e of Series 1

A molecular modelling study of **24e** was conducted with the objective of interpreting its binding interaction with BTK and correlating its potency (see experimental section 4.2.11. for docking protocol). CovDock, the covalent docking programme developed by Schrödinger, mimics the multi-step binding process of covalent modifiers by simulating both pre- and post-reactive states [120]. The crystal structure of the BTK enzyme (PDB ID: 5P9M) was obtained from the protein data bank, and the protein structure was prepared using the protein preparation wizard module of Schrödinger for docking studies. The ligands were minimised by applying an OPLS-AA force field using the ligprep module of Schrödinger [121].

Figure 13 represents the resemblance of the binding poses of **24e** (azure) and IBR (salmon pink) in the active site of BTK enzyme. At the hinge region of the BTK domain, the amino group of the pyrimidine ring of **24e** forms an H-bond with the backbone carbonyl of Glu474, while the pyrimidine ring nitrogen forms an H-bond with the backbone NH of Met477. Both IBR and **24e** evidenced important interactions with the thiol group of Cys481 of BTK, which binds covalently as Michael adducts. Through "T" shape π - π stacking, the phenoxy phenyl ring interacts with Phe540. Overall, **24e** and IBR bind to the active domain of the BTK enzyme with the same alignment, confirming its *in vitro* BTK inhibitory activity. Additional interactions of **24e** with Gln412 in the catalytic domain of the BTK enzyme are likely to contribute to BTK

inhibitory activity. IBR and **24e** docking scores were found to be -11.08 and -11.15 kcal mol⁻¹, respectively.

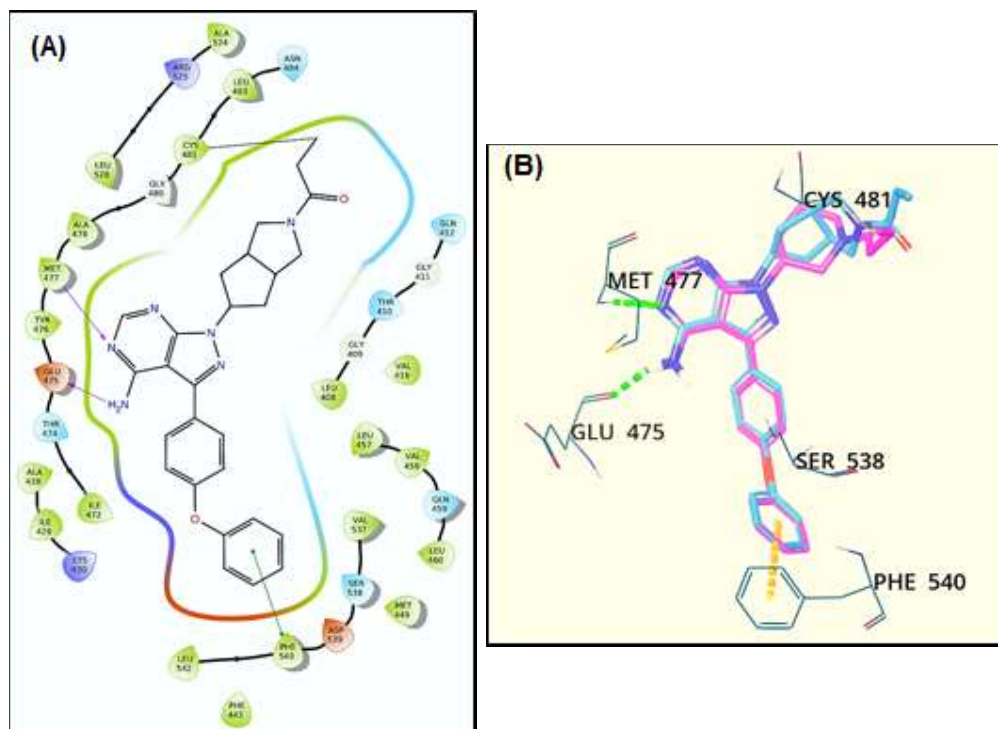


Figure 13. Docked pose of 24e within ATP active binding sites of BTK enzyme

(A) 2D ligand interaction diagram of **24e**, with residue within 5 Å, hydrogen bonds & π - π Interaction are shown with arrows and lines respectively. (B) Docked pose of **24e** and IBR superimposed (IBR is shown in with salmon pink coloured while **24e** is displayed with Azure coloured), green & orange dashed lines shows the hydrogen bonds interactions and π - π Interaction respectively.

2.3. 1-(octahydrocyclopenta[c]pyrrol-5-yl)-1H-pyrazolo[3,4-d]pyrimidin-4-amine scaffold based BTK inhibitors 32a-an (Series 2)

2.3.1. Chemistry

In preliminary research from **Series 1**, we discovered the octahydrocyclopenta[c]pyrrole analogue (**24e**) to be a superior bioisosteric alternative to piperidine, and its biological potency motivated us to make subsequent efforts to optimise the aromatic backbone component of the BTK inhibitor **24e** (Figure 14).

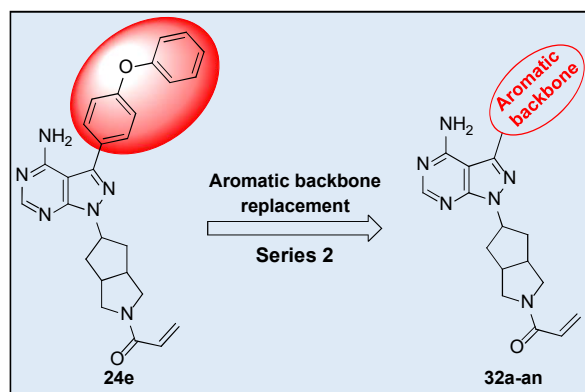


Figure 14. Designing of 1-(octahydrocyclopenta[c]pyrrol-5-yl)-1H-pyrazolo[3,4-d]pyrimidin-4-amine scaffold based BTK inhibitors 32a-an of Series 2

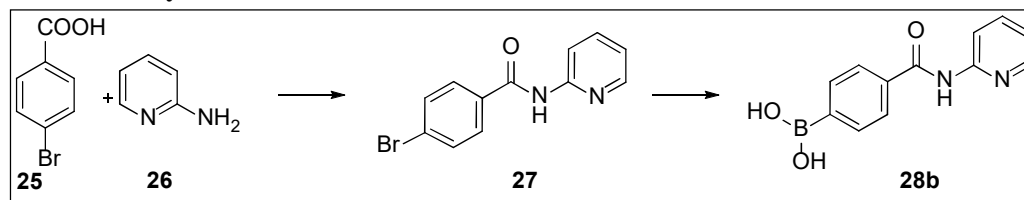
For optimisation and bioisosteric replacement of phenoxy phenyl, three sets of aromatic backbones were selected in **Series 2**. In the first set of **Series 2**, benzamide (**32a-e**, **32j-k**) and picolinamide (**32f-i**) derivatives were designed, whereas in the second set of **Series 2**, 4-phenyl ether (**32l-q**), 4-phenyl thioether (**32r-v**), and 4-phenyl alkyl (**32w-aa**) derivatives were used as the aromatic backbones. Phenyl-containing fused heterocycles (**32ab-an**) were enlisted as the aromatic backbone for the third set of **Series 2**. In total, forty compounds (**32a-an**) were synthesized in the **Series 2**, and their *in vitro* activities were evaluated.

Scheme 6 describes the synthetic route of the test compound (**32a-an**). The **scheme 5** was used to synthesise the majority of the key boronic acid intermediates. Some boronic acid intermediates were obtained from an in-house chemical library or from a commercial vendor.

Scheme 5 was utilized to prepare (4-(pyridin-2-ylcarbamoyl)phenyl)boronic acid (**28b**). EDC hydrochloride was used as a coupling agent to couple 4-bromobenzoic acid with amine. The amide product (**27**) was lithiated with *n*-BuLi before being treated with triisopropyl borate. With the addition of aqueous hydrochloric acid, the boronate product was hydrolyzed to afford a boronic acid intermediate **28b** (see experimental

section 4.1.5., for detailed procedure). Other boronic acid intermediates were also produced using the same method and the appropriate starting materials.

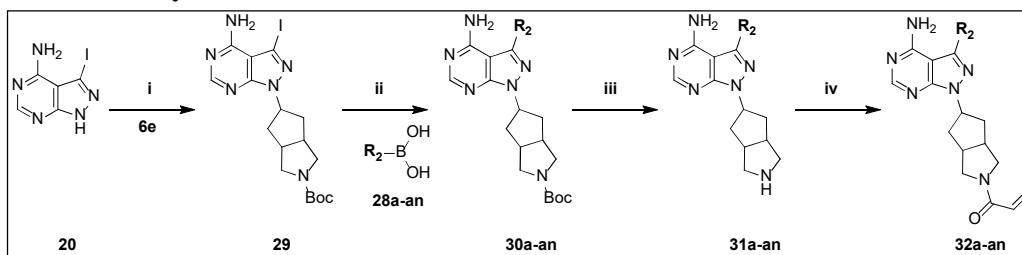
Scheme 5: Synthetic route of intermediate 28b



Reagents and conditions: i) 1-(3-Dimethylaminopropyl)-3-ethylcarbodiimide hydrochloride, 4-dimethylaminopyridine, DMF, 25°C, 18 h, 87%; ii) n-butyllithium, triisopropyl borate, THF, -50°C to 25°C, 18h, HCl(aq), 0°C to 25°C, 3h, 71%.

The synthetic route for target compounds **32a-an** is elaborated in **Scheme 6**. Iodo intermediate **20** was reacted with **6e** under Mitsunobu conditions to produce **29**, which was then reacted with various substituted boronic acids (**28a-an**) under Suzuki Miyaura cross-coupling reaction conditions to form **30a-an**. The tert-butyl carbamate group of the **30a-an** was deprotected with trifluoroacetic acid, and the resulting amines, **31a-an**, were then acylated with acryloyl chloride in the presence of base to produce the target compounds (**32a-an**). All of the target compounds were characterized by NMR, ESI-MS, UPLC, and CHN analysis. The experimental section 4.1.6. describes the procedures for preparing the target compounds, their yields, and melting points.

Scheme 6: Synthetic route of 32a-an of Series 2



Reagents and conditions: i) diisopropyl azodicarboxylate, triphenyl phosphine, THF, 25°C, 18 h, 66%; ii) R₂-boronic acid (**28a-an**), PdCl₂(PPh₃)₂, KHCO₃(aq), DMF, 90°C, 5 h, 42-76%; iii) Trifluoroacetic acid, DCM, 0°C to 25°C, 3 h, 73-92%; iv) Acryloyl chloride, N,N-Diisopropylethylamine, DCM, 0°C to 25°C, 18 h, 35-68%.

Set 1: benzamide and picolinamide-based derivatives (**R**₂)

No.	R ₂	No.	R ₂	No.	R ₂
a		e		i	
b		f		j	
c		g		k	
d		h			

Set 2: 4-phenyl ether, 4-phenyl thioether, and 4-phenyl alkyl-based derivatives (**R**₂)

No.	R ₂	No.	R ₂	No.	R ₂	No.	R ₂
l		p		t		x	
m		q		u		y	
n		r		v		z	
o		s		w		aa	

Set 3: Phenyl-containing fused heterocycle-based derivatives (**R**₂)

No.	R ₂	No.	R ₂	No.	R ₂
ab		ag		ak	
ac		ah		al	
ad		ai		am	
ae		aj		an	
af					

2.3.2. Biological evaluation of Series 2

2.3.2.1. *In vitro* BTK inhibitory and anti-proliferative activity

The *in vitro* BTK inhibitory activity of the synthesised compounds (**32a–an**) was assessed using the BTK enzyme inhibition assay, and its anti-proliferation activity was evaluated using the TMD8 cell proliferation assay (**Table 5**). The methods used in both *in vitro* assays are outlined in the experimental section 4.2.1. and 4.2.2., respectively.

Three sets of scaffolds were used to substitute the aromatic backbone of **24e** in the **Series 2**, and their IC₅₀ value was calculated in both *in vitro* experiments. The positive control, IBR, showed IC₅₀ values of 1.1 nM and 1.2 nM in the BTK enzyme and TMD8 cell proliferation assays, respectively. The majority of the benzamide derivatives (**32a–e**, **32j**, and **32k**) of the first set displayed strong inhibitory effects, whereas the most potent ones were determined to be **32b**, **32d**, and **32e**, with IC₅₀ value ≤ 1 nM in both *in vitro* assays.

When N-2-pyridyl (**32b**) was replaced with N-2-pyrazine (**32a**) or N-3-pyridyl (**32c**), BTK enzyme inhibitory activity and an anti-proliferative effect declined by four to fivefold. **32j**, which was made by adding a methyl spacer to the aromatic backbone of **32b**, demonstrated poor inhibitory activities (IC₅₀ = 55.4 and 71.3 nM) in both *in vitro* experiments. Similarly, the N-methylated aromatic backbone (**32k**) inhibited BTK enzyme (IC₅₀ = 25.7 nM) and the TMD8 cell proliferation (IC₅₀ = 33.2 nM) less efficaciously.

In comparison to the benzamide-based aromatic backbones, the picolinamide-based aromatic backbones (**32f**, **32g**, and **32h**) were slightly less potent in BTK enzyme inhibition (IC₅₀ = 8.1 nM, 7.5 nM, and 7.6 nM) and TMD8 cell proliferation (IC₅₀ = 7.2 nM, 7.1 nM, and 7.8 nM) assays.

In the second set of **Series 2**, aromatic backbones such as 4-phenyl ether, 4-phenyl thioether, and 4-phenyl alkyl-based derivatives were used to replace the phenoxyphenyl of **24e**. The few compounds with a 4-phenyl ether-based aromatic backbone (**32l–q**) that totally lack any inhibitory activities in either of the *in vitro* assays were **32l** (a morpholine analogue) and **32m** (a piperidine analogue).

However, when piperidine (**32l**) or morpholine (**32m**) was substituted with thiophenyl (**32n**, $IC_{50} = 11.2$ nM and 12.7 nM, in BTK enzyme and TMD8 cell proliferation assays, respectively), the inhibitory activities were significantly enhanced. The *in vitro* inhibitory activities were sustained even though thiophenyl was replaced with thioethyl (**32o**) or thio isopropyl (**32q**). **32p**, the sulfonyl analogue of **32o**, showed drastically less inhibition of the BTK enzyme ($IC_{50} = 89$ nM) and the TMD8 cell proliferation ($IC_{50} = 82$ nM).

The 4-phenyl thioether based aromatic backbones (**32r–u**) showed good potency in both *in vitro* assays, among them, the analogues of propyl sulfane (**32u**) and ethyl sulfane (**32v**) were found to be highly potent in BTK enzyme inhibition ($IC_{50} = 0.8$ nM and 0.8 nM, respectively), as well as in TMD8 cell proliferation ($IC_{50} = 0.4$ nM and 1.7 nM, respectively) assays. However, its corresponding analogues, propyl ether (**32r**) and ethyl ether (**32s**), showed weaker inhibition of the BTK enzyme ($IC_{50} = 10.4$ nM and 9.4 nM, respectively) and the TMD8 cell proliferation ($IC_{50} = 10.8$ nM and 8.5 nM, respectively). This emphasizes the significance of the sulfane moiety. As expected, when sulfane (**32u**) was oxidized to sulfonyl (**32t**), its *in vitro* potency decreased ($IC_{50} = 18.9$ nM in BTK enzyme and 13.7 nM in TMD8 cell proliferation).

The BTK enzyme inhibition and anti-proliferation activity of aromatic backbones based on 4-phenyl alkyl (**32w–aa**) was very weak. With an IC_{50} value of 6.0 nM in the BTK

enzyme and 2.3 nM in the TMD8 cell proliferation assay, **32x** was the most potent of the 4-phenyl alkyl-based derivatives. **32z** and **32aa** displayed IC₅₀ values of 62.5 nM and 10.5 nM in the BTK enzyme inhibition assay, and 82.4 nM and 10.9 nM in the assay using the TMD8 cell proliferation, respectively. **32w** or **32y** failed to inhibit the BTK enzyme or the TMD8 cell proliferation.

Compounds **32ab-an** were synthesized using specific phenyl-containing heterocycles, and a total of thirteen compounds were produced in the third set of **Series 2** for the aromatic backbone optimization. The loss of BTK enzyme inhibitory and anti-proliferative activities of **32ab**, **32af**, **32ai**, and **32aj** could be related to their inability to fit into the backside pocket of Thr474 of BTK.

32ad, **32ae**, and **32an** were moderately active in the BTK enzyme inhibition assay, with IC₅₀ values ranging from 25 nM to 55 nM, whereas in the anti-proliferation assay, the IC₅₀ value varied from 25 nM to 60 nM. With IC₅₀ values of 6.6 nM and 6.8 nM, the aromatic backbone of benzothiophene (**32ac**) was found to have strong inhibitory activities. Additionally, when the thiophene ring was made saturated (**32al**), the alteration enhanced BTK enzyme inhibition (IC₅₀ = 4.0 nM) and anti-proliferation activity (IC₅₀ = 3.5 nM). In BTK enzyme and TMD8 cell proliferation assays, the aromatic backbone of Methylenedioxybenzene (**32am**) had IC₅₀ values of 11.7 nM and 9.3 nM, respectively, but the inhibitory activity was drastically decreased when the Methylene was substituted with Difluoromethylene (**32am**, IC₅₀ = 51.1 nM and >100 nM, in BTK enzyme and TMD8 cell proliferation assay, respectively).

Along with the benzothiophene moiety, the third set also comprised aromatic backbones based on prenyloxadiazole (**32ah**, IC₅₀ = 5.6 nM and 7.1 nM, in BTK enzyme and TMD8 cell proliferation assay, respectively) and phenylbenzoxazole

(**32am**, IC_{50} = 5.6 nM and 8.7 nM, in BTK enzyme and TMD8 cell proliferation assay, respectively), and both of them demonstrated potent inhibitory effects.

Table 5. *In vitro* BTK enzyme and TMD8 cell proliferation inhibitory data of **32a-an** of Series 2

Comp.	R ₂	BTK IC ₅₀ (nM) ^a	TMD8 IC ₅₀ (nM) ^b	Comp.	R ₂	BTK IC ₅₀ (nM) ^a	TMD8 IC ₅₀ (nM) ^b
32a		4.4	4.3	32u		0.8	0.4
32b		1.0	0.8	32v		0.8	1.7
32c		4.0	3.9	32w		>100	>100
32d		0.6	0.4	32x		6.0	2.3
32e		0.6	0.2	32y		>100	>100
32f		8.1	7.2	32z		62.5	82.4
32g		7.5	7.1	32aa		10.5	10.9
32h		7.6	7.8	32ab		>100	>100
32i		68.5	79.2	32ac		6.6	6.8
32j		55.4	71.3	32ad		41.3	59.5
32k		25.7	33.2	32ae		18	26.9
32l		>100	>100	32af		>100	>100
32m		>100	>100	32ag		38	46.2
32n		11.7	12.7	32ah		5.6	7.1
32o		8.3	8.8	32ai		>100	>100

32p		89	82	32aj		>100	>100
32q		14.6	7.5	32ak		5.6	8.7
32r		10.4	10.8	32al		4.0	3.5
32s		9.4	8.5	32am		11.7	9.3
32t		18.9	13.7	32an		51.1	>100
	IBR	1.1	1.2				

All the data are shown as the mean for three experiments. ^a BTK inhibition (IC₅₀) determination using *in vitro* BTK kinase assay on ADP Glo platform, ^b TMD8 cytotoxicity inhibition (IC₅₀) determination using TMD8 cell lines assay.

32b, 32d, 32e, 32u, and 32v from **Series 2** were discovered to be highly potent in the BTK enzyme and TMD8 cell proliferation assays, and their potency was comparable to that of IBR. Hence, **32b, 32d, 32e, 32u, and 31v** were selected for CYP and hERG inhibition studies.

2.3.2.2. CYP and hERG inhibitory activities of the lead compounds of Series 2

The selected test compound (**32b, 32d, 32e, 32u, and 32v**) of **Series 2** was incubated with human liver microsomes and NADPH in the presence of CYP-specific substrates to evaluate CYP inhibitory activities (see experimental section 4.2.3. for detail procedures). The automated patch clamp assay was used to assess hERG inhibitory activities. At 10 μ M concentration (see experimental section 4.2.4. for detail procedures), In **Table 6**, the results are presented.

Tested compounds (**32b, 32d, 32u, and 32v**) showed <50% inhibition of hERG at 10 μ M concentration, except for **32e**, which showed 63% inhibition. CYP inhibition study data reveals that the phenyl thio-ether analogues **32u** and **32v** inhibit multiple CYP isoforms (>50% inhibition of 2C8, 2C9, 2D6, and 2C19) at 10 μ M concentration. Whereas, the benzamide analogue **32b** showed no CYP liabilities (<50% inhibition) at

10 μ M concentration, while **32d** and **32e** showed >50% inhibition of 2C9 at 10 μ M concentration. In general, CYP inhibition has also been correlated with increased molecular weight (MW) and lipophilicity. Among **32b**, **32d**, and **32e**, only **32b** was found to be devoid of CYP liability, which could be correlated with its low MW and Log P. Compounds **32u** and **32v** exhibit higher Log P (3.63 and 3.86, respectively) and lower basicity compared to **32b**, which may account for multiple CYP inhibitions.

Table 6. CYP and hERG inhibitory activity of the lead compounds of Series 2

Comp.	%hERG ^a inhibition @ 10 μ M	% CYP inhibition ^b @ 10 μ M					
		CYP1A2	CYP2C8	CYP2C9	CYP2D6	CYP2C19	CYP3A4
32b	NI	NI	12	19	17	1	12
32d	26	13	27	63	34	27	2
32e	63	NI	63	79	27	38	33
32u	32	18	75	79	60	63	63
32v	44	12	72	58	69	50	40
IBR	35	NI	81	86	31	39	55

^a In the automated patch clamp assay, ^b incubated test compound with human liver microsomes and NADPH in the presence of CYP specific substrate, value are mean of three repeat experiment, NI = No inhibition.

2.3.2.3. Pharmacokinetic studies of **32b** of Series 2

32b demonstrated excellent *in vitro* activity and also was found to be devoid of CYP and hERG liabilities. Therefore, **32b** was subjected to an *in vivo* PK study in male BALB/c mice and Wister rats. In single-dose PK studies (3 mg/kg, po, and 1 mg/kg, iv) of **32b** and comparator (IBR), various PK parameters (T_{max} , C_{max} , $T_{1/2}$, Cl, AUC, and %F) were recorded (**Table 7**). The absolute oral bioavailability (%F) of **32b** (3 mg/kg) in mice was found to be 47%, with a C_{max} of 703 ng/mL at 0.25 h (T_{max}), an AUC of 590 ng.h/mL and a half-life ($T_{1/2}$) of 0.76 hours. The %F of **32b** in rats was found to be 75%, with a C_{max} of 650 ng/mL, an AUC of 908 ng.h/mL and a $T_{1/2}$ of 2.2 hours. Thus,

among the compounds tested, **32b** revealed a comparatively better PK profile than **24e**, and IBR.

Table 7. Pharmacokinetic profile^a of 32b

Dose	Parameters	32b		IBR	
		<i>Mice</i>	<i>Rat</i>	<i>Mice</i>	<i>Rat</i>
IV 1 mg kg ⁻¹	AUC (ng.h/mL)	422	479	151	250
	V _{ss} (L/kg)	0.70	0.88	0.50	1.50
	CL (ml/min/kg)	39.5	36.0	27.5	66.3
	T _{1/2} (h)	0.40	0.60	0.20	0.40
PO 3 mg kg ⁻¹	T _{max} (h)	0.25	0.25	0.25	0.25
	C _{max} (ng/mL)	703	794	402	129
	AUC (ng.h/mL)	588	1074	277	86
	T _{1/2} (h)	0.80	2.00	0.30	0.80
	%F*	47	75	15	11

^a In male BALB/c mice and male Wister rats (n = 3), compounds were administered orally (po) at 3 mg/kg dose and plasma concentration was analyzed by LC-MS, values indicate Mean.

*Oral bioavailability (%F) was calculated wrt to iv AUC. Test Compounds were administered at 1 mg/kg dose.

2.3.3. Molecular docking study of 32b of Series 2

A molecular modelling study of **32b** was conducted with the objective of interpreting its binding interaction with BTK and correlating its potency. CovDock, the covalent docking programme developed by Schrödinger, mimics the multi-step binding process of covalent modifiers by simulating both pre- and post-reactive states (see experimental section 4.2.11. for detailed protocol). The crystal structure of the BTK enzyme (PDB ID: 5P9M) was obtained from the protein data bank, and the protein structure was prepared using the protein preparation wizard module of Schrödinger for docking studies. The ligands were minimised by applying an OPLS-AA force field using the ligprep module of Schrödinger.

The binding orientations of **32b** (azure) and IBR (salmon pink) in the active site of the BTK enzyme are the same, as shown in **Figure 15**. The pyrimidine ring nitrogen forms an H-bond with the backbone NH of Met477 in the hinge region of the BTK domain,

while the amino group of the pyrimidine ring **32b** forms an H-bond with the backbone carbonyl of Glu474. With the thiol group of Cys481 in BTK, which binds covalently as Michael adducts, both IBR and **32b** revealed significant interactions. Through "T" shape π - π stacking, the N-2-pyridyl ring interacts with Phe540. Eventually, **32b** and IBR have the same alignment when they bind to the active domain of the BTK enzyme, establishing their *in vitro* BTK inhibitory activity. An additional bonding of **32b** in the catalytic domain of BTK enzyme with Ser538 and Gln412 is believed to be contributing to its potent BTK inhibitory activity. The docking scores of IBR and **32b** were -11.08 and -11.89 kcal/mol, respectively.

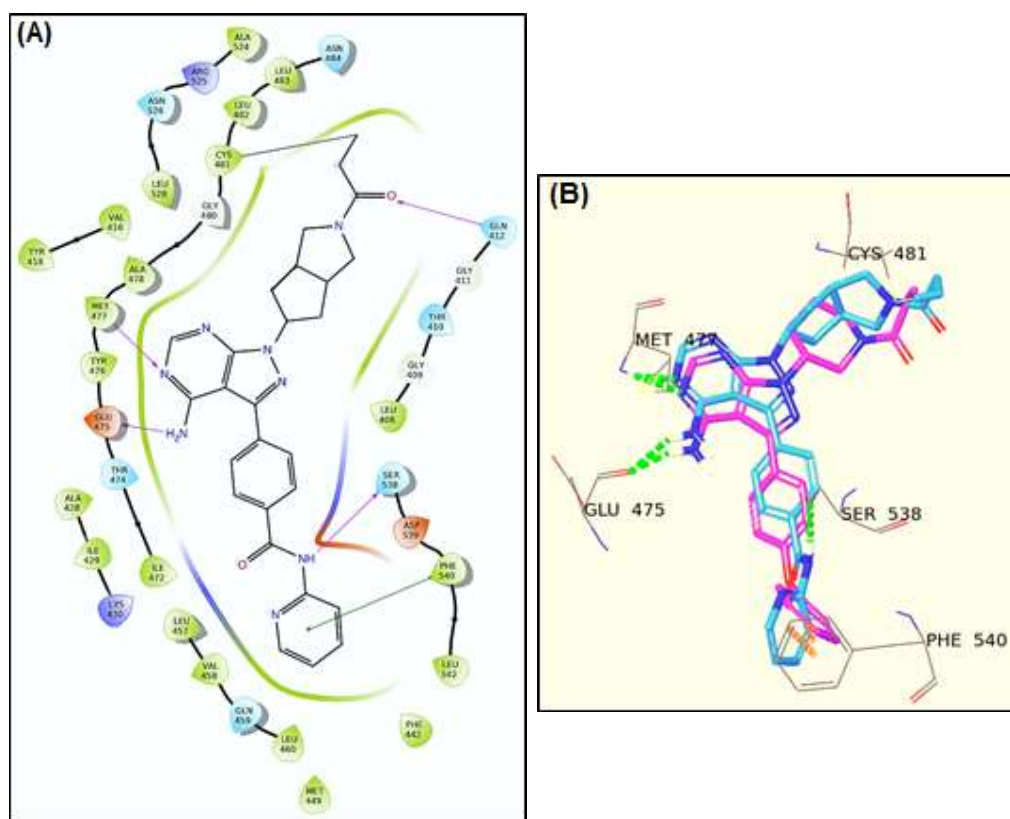


Figure 15. Docked pose of 32b within ATP active binding sites of BTK enzyme
(A) 2D ligand interaction diagram of **32b**, with residue within 5 Å, hydrogen bonds & π - π Interaction are shown with arrows and lines respectively. **(B)** Docked pose of **32b** and IBR superimposed (IBR is shown in with salmon pink coloured while **32b** is displayed with Azure coloured), green & orange dashed lines shows the hydrogen bonds interactions and π - π Interaction respectively.

2.4. 4-(4-amino-1-(octahydrocyclopenta[c]pyrrol-5-yl)-1H-pyrazolo[3,4-d]pyrimidin-3-yl)-N-(pyridin-2-yl)benzamide scaffold based BTK inhibitors **32ao-av** (Series 3)

2.4.1. Chemistry

The nucleophilic Cys481 of the BTK enzyme interacts covalently with electrophilic warheads, which is an essential component of BTK inhibitor structures. **32b** of **Series 2** was found to be highly potent (BTK enzyme and TMD8 cell proliferation assays, IC₅₀ values of 1.0 and 0.8 nM, respectively) and devoid of hERG and CYP liabilities (<50% inhibition at 10 μ M concentration) when using a conventional acrylamide warhead. To study the influence of warheads on *in vitro* activity, selected Michael acceptors and other moiety (R₃, **Table 8**) were used as warheads instead of acrylamide, and eight compounds **32ao-av** were synthesized in **Series 3** (**Figure 16**).

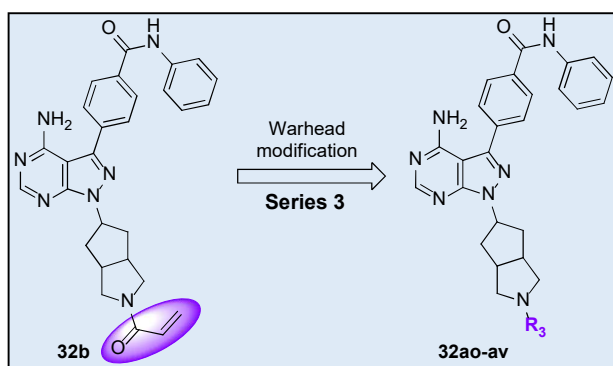
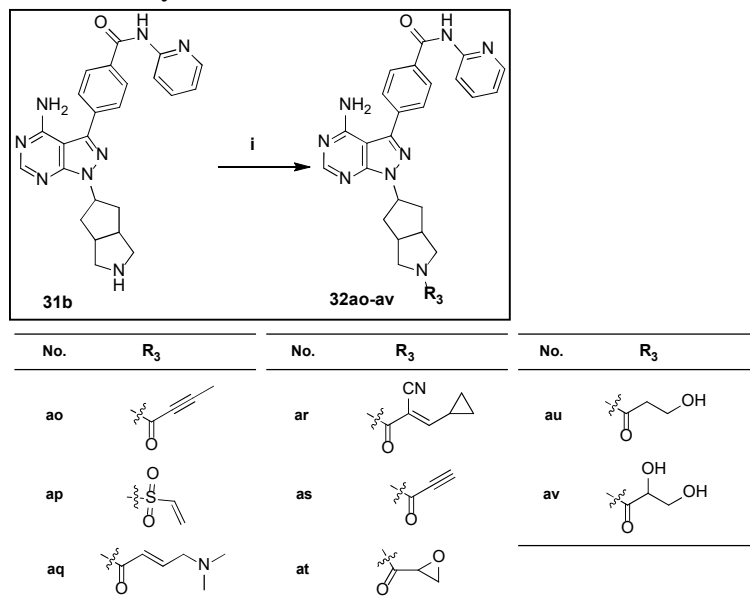


Figure 16. Designing of 4-(4-amino-1-(octahydrocyclopenta[c]pyrrol-5-yl)-1H-pyrazolo[3,4-d]pyrimidin-3-yl)-N-(pyridin-2-yl)benzamide scaffold based BTK inhibitors **32ao-av** of **Series 3**

The synthetic route for the preparation of target compounds **32ao-av** was displayed in **Scheme 7**. Intermediate **31b** was coupled with various acyl chloride in the presence of base triethylamine or corresponding acid was used with HBTU as a coupling reagent to provide the targeted compounds **32ao-av**. All of the target compounds were characterized by NMR, ESI-MS, UPLC, and CHN analysis. The experimental section

4.1.7. describes the procedures for preparing the target compounds, their yields, and melting points.

Scheme 7: Synthetic route of 32ao-av of Series 3



Reagents and conditions: i) R₃-Acid, O-(1H-Benzotriazol-1-yl)-N,N,N',N'-tetramethyluronium hexafluorophosphate, N,N-Diisopropylethylamine, DMF, 0°C to 25°C, 18 h, 42-71%;

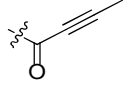
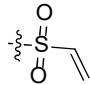
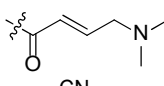
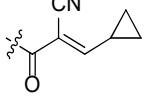
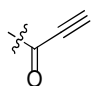
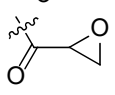
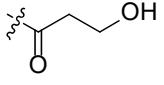
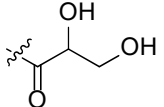
2.4.2. Biological evaluation of Series 3

2.4.2.1. *In vitro* BTK inhibitory and anti-proliferative activity

In **Series 3**, SAR study around various α , β -unsaturated amide groups reveals that among the eight different warheads selected (**Table 8**), only butynamide (**32ao**) matched with the acrylamide (**32b**) in the BTK and TMD8 assays, with IC₅₀ values of 1.2 nM and 0.9 nM, respectively. Favourable butynamide warhead is also present in Acalabrutinib and Tirabrutinib, with pyrrolidine linker. Other Michael acceptors like **32ap** (vinyl sulfonamide), **32aq** (dimethyl aminomethyl amide), and **32as** (2-propionyl amide) displayed four to six fold less potency in both the *in vitro* assays, while **32ar** (cyano cyclopropyl acrylamide) and **32at** (epoxide carboxamide) showed poor BTK enzyme inhibitory and anti-proliferative effects. **32au** (3-hydroxy propanamide) and **32av** (2,3-dihydroxy propanamide) lost BTK enzyme inhibitory activity due to the

absence of the α , β -unsaturated amide group. Thus, it has been observed that only acrylamide and butynamide warheads containing compounds (**32b** and **32ao**) retained potent inhibitory activity in the both *in vitro* assays. This could be due to cyclopentyl pyrrole linker, which may provide optimal spatial angle, specifically with these two warheads only so that these warheads can interact covalently with Cys481. It appears that extended warheads such as dimethyl amino methyl amide (**32aq**), cyano cyclopropyl acrylamide (**32ar**) and 2-propioloyl amide (**32as**) are not favourable with cyclopentyl pyrrole linker, which could be due to extra spacing imparted by cyclopentyl pyrrole linker.

Table 8. *In vitro* BTK enzyme and TMD8 cell proliferation inhibitory data of 32ao-av of Series 3

Comp.	R ₃	BTK IC ₅₀ (nM) ^a	TMD8 IC ₅₀ (nM) ^b
32ao		1.2	0.9
32ap		4.9	3.9
32aq		5.2	4.7
32ar		>100	83
32as		6.2	5.8
32at		48.2	61.4
32au		>100	>100
32av		>100	>100
	IBR	1.1	1.2

All the data are shown as the mean for three experiments. ^a BTK inhibition (IC₅₀) determination using *in vitro* BTK kinase assay on ADP Glo platform, ^b TMD8 cytotoxicity inhibition (IC₅₀) determination using TMD8 cell lines assay.

2.4.2.2. CYP and hERG inhibitory activities of the lead compound of Series 3

From **series 3**, **32ao** was selected for CYP and hERG inhibitory studies since it was found to be the most potent compound in *in vitro* BTK inhibitory and anti-proliferative activity. **32ao** was incubated with human liver microsomes and NADPH in the presence of CYP-specific substrates to evaluate CYP inhibitory activities (see experimental section 4.2.3. for detail procedures). The automated patch clamp assay was used to assess hERG inhibitory activities. At 10 μ M concentration (see experimental section 4.2.4. for detail procedures), In CYP and hERG inhibitory studies, **32ao** showed less than 50% inhibition for all CYP isoenzymes and hERG inhibition at 10 μ M concentration (**Table 9**).

Table 9. CYP and hERG inhibitory activity of the lead compound of Series 3

Comp.	%hERG ^a inhibition @ 10 μ M	% CYP inhibition ^b @ 10 μ M					
		CYP1A2	CYP2C8	CYP2C9	CYP2D6	CYP2C19	CYP3A4
32ao	23	NI	NI	28	15	18	16
IBR	35	NI	81	86	31	39	55

^a In the automated patch clamp assay, ^b incubated test compound with human liver microsomes and NADPH in the presence of CYP specific substrate, value are mean of three repeat experiment, NI = No inhibition.

2.4.2.3. Pharmacokinetic studies of 32ao of Series 3

In **Series 3**, compound **32ao** was found to be most potent and devoid of CYP and hERG liabilities, so it was selected for considered for an *in vivo* PK study. PK of Compound **32ao** was assessed using male BALB/c mice and Wister rats (see experimental section 4.2.5. for detail procedures). In single-dose PK studies (3 mg/kg, po, and 1 mg/kg, iv) of **32ao** and comparator (IBR), various PK parameters (T_{max} , C_{max} , $T_{1/2}$, Cl, AUC, and %F) were recorded (**Table 10**). The absolute oral bioavailability (%F) of **32ao** (3 mg/kg) in mice was found to be 37%, with a C_{max} of 368 ng/mL at 0.25 h (T_{max}), an

AUC of 300 ng.h/mL and a half-life ($T_{1/2}$) of 0.67 hours. The %F of **32ao** in rats was found to be 31%, with a C_{max} of 396 ng/mL, an AUC of 219 ng.h/mL and a $T_{1/2}$ of 0.80 hours. Thus, among the compounds tested, **32ao** revealed a comparatively better PK profile than **24e**, and IBR. Although **32ao** has a slightly inferior PK profile compared to **32b**.

Table 10. Pharmacokinetic profile^a of 32ao

Dose	Parameters	32ao		IBR	
		<i>Mice</i>	<i>Rat</i>	<i>Mice</i>	<i>Rat</i>
IV 1 mg kg ⁻¹	AUC (ng.h/mL)	270	236	151	250
	V _{ss} (L/kg)	0.70	0.54	0.50	1.50
	CL (ml/min/kg)	44.3	42.1	27.5	66.3
	$T_{1/2}$ (h)	0.29	0.31	0.20	0.40
PO 3 mg kg ⁻¹	T_{max} (h)	0.25	0.25	0.25	0.25
	C_{max} (ng/mL)	368	396	402	129
	AUC (ng.h/mL)	300	219	277	86
	$T_{1/2}$ (h)	0.67	0.80	0.30	0.80
	%F*	37	31	15	11

^aIn male BALB/c mice and male Wister rats (n = 3), compounds were administered orally (po) at 3 mg/kg dose and plasma concentration was analyzed by LC-MS, values indicate Mean.

*Oral bioavailability (%F) was calculated wrt to iv AUC. Test Compounds were administered at 1 mg/kg dose.

2.4.3. Molecular docking study of 32ao of Series 3

A molecular modelling study of **32ao** was conducted with the objective of interpreting its binding interaction with BTK and correlating its potency. CovDock, the covalent docking programme developed by Schrödinger, mimics the multi-step binding process of covalent modifiers by simulating both pre- and post-reactive states (see experimental section 4.2.11. for detailed protocol). The crystal structure of the BTK enzyme (PDB ID: 5P9M) was obtained from the protein data bank, and the protein structure was prepared using the protein preparation wizard module of Schrödinger for docking studies. The ligands were minimised by applying an OPLS-AA force field using the ligprep module of Schrödinger.

Molecular docking study shows that **32ao** and IBR adopts similar conformation in the active site of the BTK enzyme (**Figure 17**). The pyrimidine ring nitrogen forms an H-bond with the backbone NH of Met477 in the hinge region of the BTK domain, while the amino group of the pyrimidine ring **32ao** forms an H-bond with the backbone carbonyl of Glu474. With the thiol group of Cys481 in BTK, which binds covalently as Michael adducts, both IBR and **32ao** revealed significant interactions. The additional interactions that **32ao** has with Ser538 in the active domain of the BTK enzyme describe its potent BTK inhibitory activity. The docking scores of IBR and **32ao** were -11.08 and -11.62 kcal/mol, respectively.

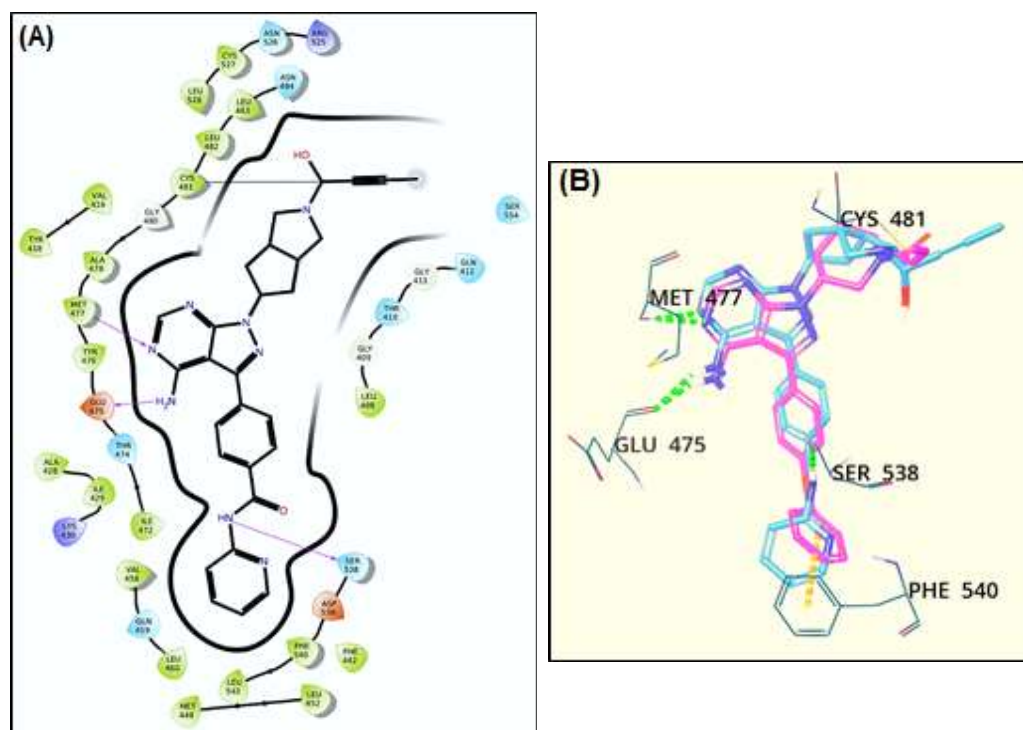


Figure 17. Docked pose of 32ao within ATP active binding site of BTK enzyme

(A) 2D ligand interaction diagram of **32ao**, with residue within 5 Å, hydrogen bonds and π - π Interaction are shown with arrows and lines respectively. (B) Docked pose of **14ao** and IBR superimposed (IBR is shown in with salmon pink coloured while **32ao** is displayed with Azure coloured), green & orange dashed lines shows the hydrogen bonds interactions and π - π Interaction respectively.

2.5. BTK inhibitors (41, 42, 51, 52, 61, 62, 71, and 72) based on pyrazolo-pyrimidin-4-amine scaffold's mimetic aromatic heterocycles (Series 4)

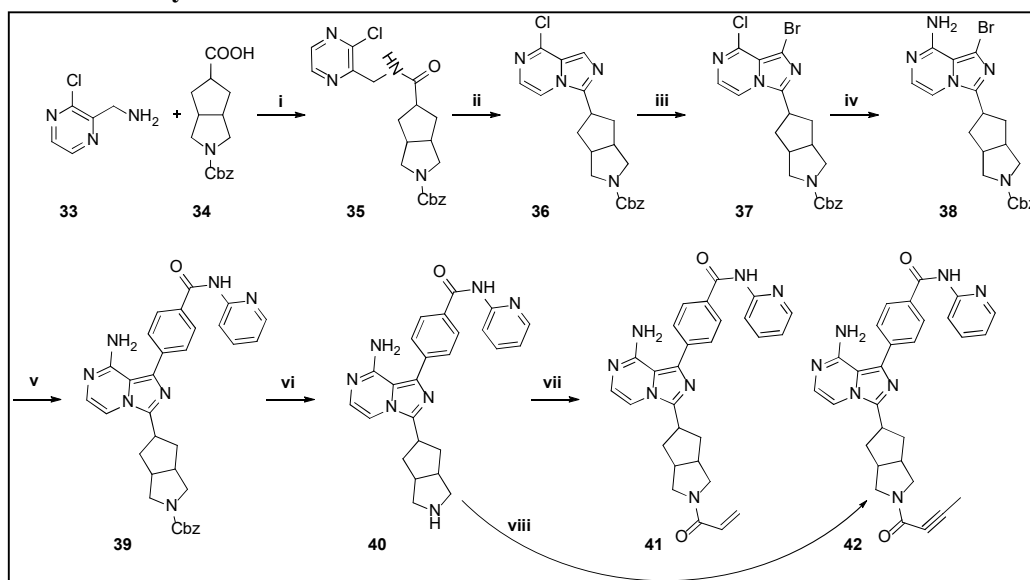
2.5.1. Chemistry

Pyrazolo-pyrimidine is a key pharmacophore of Pyrazolo-pyrimidin-4-amine-based BTK inhibitors and it interacts with the hinge region of BTK enzyme through the hydrogen bonding. It also provides orientation to the aromatic backbone and linker, which create a "Y" shape that is essential for BTK inhibitory activities. In the present **Series 4**, we intended to incorporate mimetic heterocycles of Pyrazolo-pyrimidine, such as Pyrrolo-pyrimidin, Oxo-purine, Imidazo-pyrazine, and Pyrazole scaffolds, in place of Pyrazolo-pyrimidine. The aromatic backbone of N-2-pyridylbenzamide and the amine linker of octahydrocyclopenta[c]pyrrol were preserved, while acrylamide and butynamide were utilized as a warhead in the **Series 4** to synthesize eight target compounds (**41**, **42**, **51**, **52**, **61**, **62**, **71**, and **72**), which were evaluated for *in vitro* BTK inhibitory and anti-proliferative activity. The synthetic routes for the target molecules are described in **Schemes 8, 9, 10, 11, and 12**. All of the target compounds were characterized by NMR, ESI-MS, UPLC, and CHN analysis. The experimental section 4.1.8., 4.1.9., 4.1.10., and 4.1.11. describes the procedures for preparing the target compounds, their yields, and melting points.

In general, Target molecules **41** and **42** were synthesized in accordance with **Scheme 8**. (3-chloropyrazin-2-yl)methanamine was reacted with 2-((benzyloxy)carbonyl)octahydrocyclopenta[c]pyrrole-5-carboxylic acid using HBTU as a coupling agent, and obtained amide product (**35**) was heated with phosphorus oxychloride to get an imidazo[1,5-a]pyrazin ring (**36**). Intermediate **36** was brominated with N-bromosuccinimide to yield intermediate **37**. The chloro to amine transformation

was achieved by heating **37** with aqueous ammonia in a sealed tube, followed by being subjected to a Suzuki-Miyaura coupling reaction with 4-(pyridin-2-ylcarbamoyl)phenyl)boronic acid to produce **39**, and subsequent deprotection of benzyl carbamate under hydrogenation gives **40**. The target compounds **41** and **42** were obtained by coupling of amine (**40**) with acryloyl chloride and but-2-ynoic acid, respectively (see experimental section 4.1.8. for detailed procedures).

Scheme 8: Synthetic route of 41 and 42 of Series 4

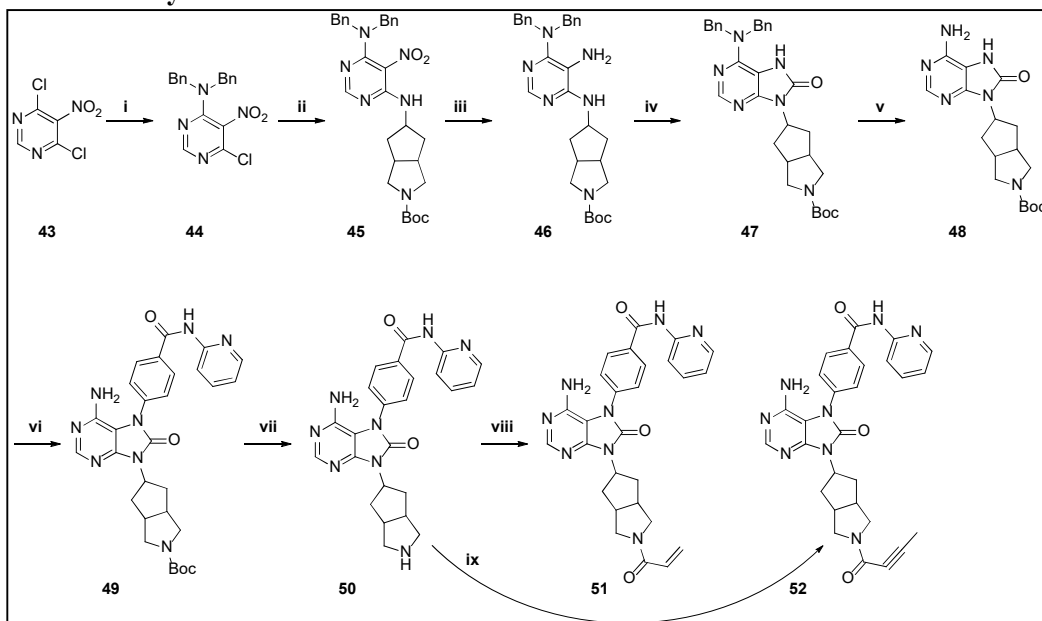


Reagents and conditions: i) O-(1H-Benzotriazol-1-yl)-N,N,N',N'-tetramethyluronium hexafluorophosphate, N,N-Diisopropylethylamine, DMF, 25°C, 16 h, 78%; ii) Phosphorus oxychloride, DMF_(cat), ACN, 75 °C, 4 h, 61%; iii) N-bromosuccinimide, DMF, 25°C, 5 h, 89%; iv) Aqueous ammonia, 2-butanol, 90°C, 17 h, 81%; v) (4-(pyridin-2-ylcarbamoyl)phenyl)boronic acid, PdCl₂(PPh₃)₂, KHCO_{3(aq)}, DMF, 90°C, 8 h, 68%; vi) Pd/C, H_{2(g)}, MeOH, 25°C, 2 h, 91%; vii) Acryloyl chloride, N,N-Diisopropylethylamine, DCM, 0°C to 25°C, 18 h, 62% viii) but-2-ynoic acid, O-(1H-Benzotriazol-1-yl)-N,N,N',N'-tetramethyluronium hexafluorophosphate, N,N-Diisopropylethylamine, DMF, 0°C to 25°C, 18 h, 73%.

The target molecules **51** and **52** were synthesized following **Scheme 9**. Nucleophilic substitution of 4,6-dichloro-5-nitropyrimidine with dibenzylamine provided the **44**, which was heated with tert-butyl 5-aminohexahydrocyclopenta[c]pyrrole-2(1H)-carboxylate in the presence of pyridine to give the **45**. Iron metal and ammonium chloride were used to reduce the nitro intermediate (**45**) to diamine (**46**), and the

resulting diamine (**46**) was then treated with triphosgene to form **47**. Intermediate **47** was debenzylated employing palladium-catalyzed hydrogenation, and the resulting **48** was subjected to copper acetate-promoted modified Chan–Lam coupling with (4-(pyridin-2-ylcarbamoyl)phenyl)boronic acid. The Boc deprotection of **49** using trifluoroacetic acid provided an amine intermediate (**50**). Acryloyl chloride was used to acylate an amine (**50**) to produce target compound **51**, whereas but-2-ynoic acid and an amine (**50**) were coupled to get target compound **52** (see experimental section 4.1.9. for detailed procedures).

Scheme 9: Synthetic route of 51 and 52 of Series 4

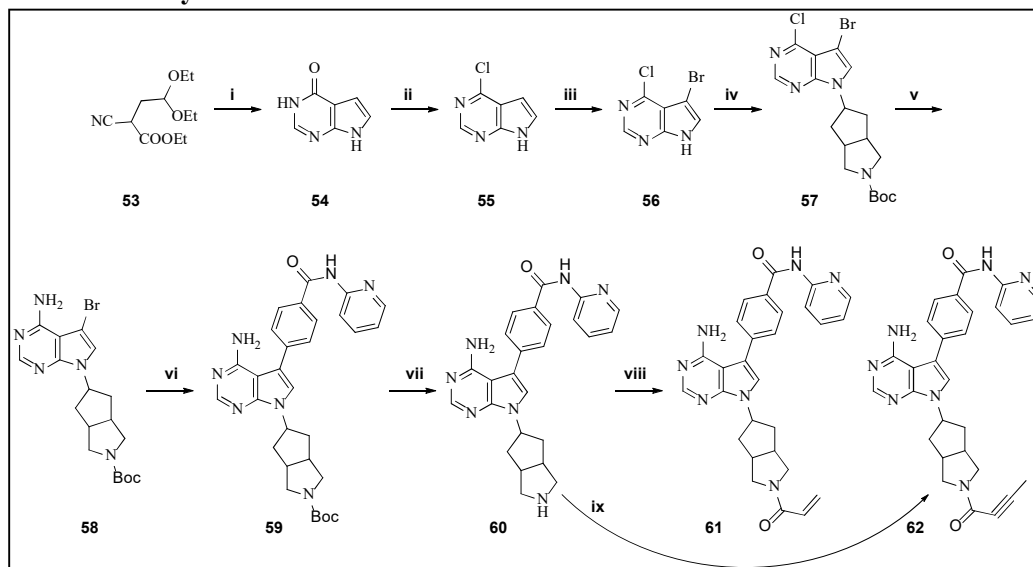


Reagents and conditions: i) Dibenzylamine, DMF, 25°C, 18 h, 85%; ii) Tert-butyl 5-amino-1H-pyrrole-2-carboxylate, pyridine, 1,4 dioxane, 80°C, 5 h, 78%; iii) Iron, ammonium chloride, EtOH, H₂O, 80°C, 2 h, 84%; iv) triphosgene, triethylamine, DCM, 25°C, 3 h, 58%; v) Pd/C, H₂(g), MeOH, 80%; vi) (4-(pyridin-2-ylcarbamoyl)phenyl)boronic acid, anhydrous copper(II) acetate, pyridine, DCM, 25°C, 48 h, 54%; vii) Trifluoroacetic acid, DCM, 0°C to 25°C, 3 h, 92%; viii) Acryloyl chloride, N,N-Diisopropylethylamine, DCM, 0°C to 25°C, 18 h, 62%; ix) but-2-ynoic acid, O-(1H-Benzotriazol-1-yl)-N,N,N',N'-tetramethyluronium hexafluorophosphate, N,N-Diisopropylethylamine, DMF, 0°C to 25°C, 18 h, 71%.

The synthetic routes for preparation of **61** and **62** were depicted in **Scheme 10**. Ethyl 2-cyano-4,4-diethoxybutanoate and Formamidine acetate were warmed with sodium ethoxide and then treated with hydrochloric acid to get **55**. 4-chloro-4a,7a-dihydro-7H-

pyrrolo[2,3-d]pyrimidine (**56**) was yielded by heating **55** with phosphorus oxychloride, and it was then brominated by N-bromosuccinimide. **57** was formed by reacting **56** with tert-butyl 5-((methylsulfonyl)oxy)hexahydrocyclopenta[c]pyrrole-2(1H)-carboxylate. The chloro to amine transformation was achieved by heating **57** with aqueous ammonia in a sealed tube, followed by being subjected to a Suzuki-Miyaura cross-coupling reaction with (4-(pyridin-2-ylcarbamoyl)phenyl)boronic acid to obtain **59**. The Boc deprotection of **59** using trifluoroacetic acid provided an amine intermediate (**60**). Acryloyl chloride was used to acylate an amine (**60**) to produce target compound **61**, whereas but-2-ynoic acid and an amine (**60**) were coupled to get target compound **62** (see experimental section 4.1.10. for detailed procedures).

Scheme 10: Synthetic route of 61 and 62 of Series 4

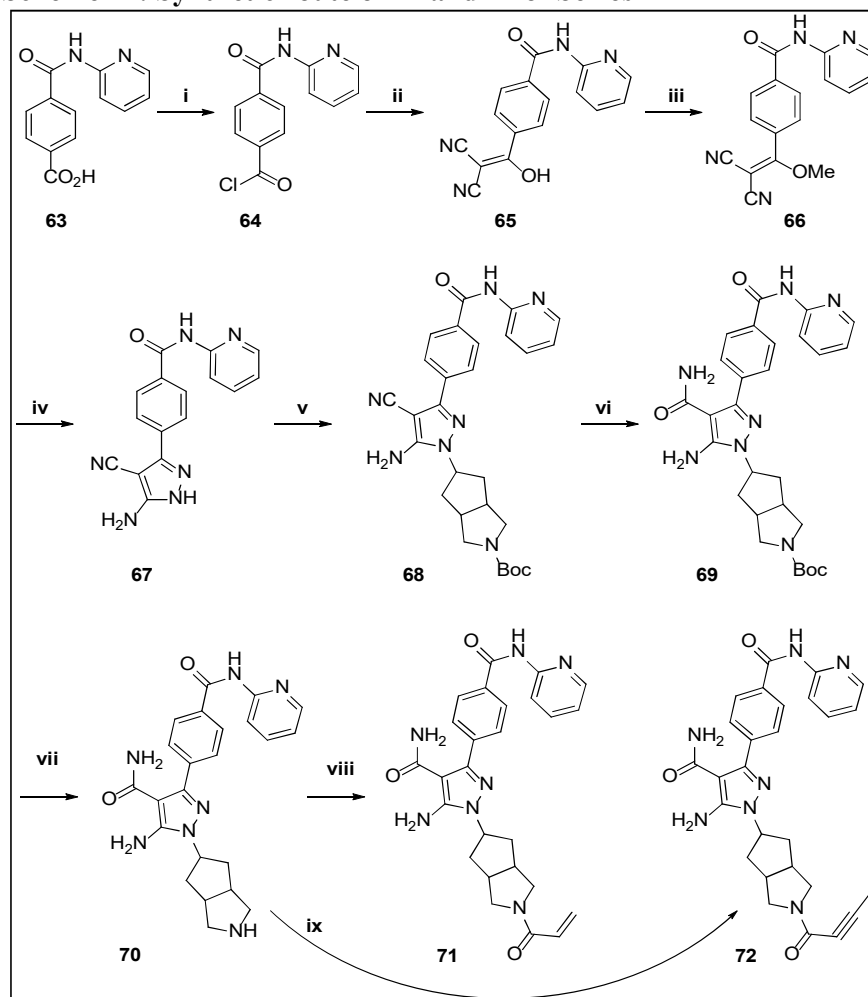


Reagents and conditions: i) Sodium ethoxide, Formamidine acetate, EtOH, 6N HCl_(aq), 45°C, 8 h, 54%; ii) Phosphorus oxychloride, 105°C, 2 h, 78%; iii) N-bromosuccinimide, DMF, 25°C, 2 h, 92%; iv) Tert-butyl 5-((methylsulfonyl)oxy)hexahydrocyclopenta[c]pyrrole-2(1H)-carboxylate, cesium carbonate, DMF, 90°C, 2 h, 58%; v) Aqueous ammonia, 1,4 Dioxane, 120°C, 16 h, 72%; vi) (4-(pyridin-2-ylcarbamoyl)phenyl)boronic acid, PdCl₂(PPh₃)₂, KHCO_{3(aq)}, DMF, 80°C, 3 h, 86%; vii) Trifluoroacetic acid, DCM, 25°C, 5 h, 90%; viii) Acryloyl chloride, N,N-Diisopropylethylamine, DCM, 0°C to 25°C, 18 h, 67%; ix) but-2-ynoic acid, O-(1H-Benzotriazol-1-yl)-N,N,N',N'-tetramethyluronium hexafluorophosphate, N,N-Diisopropylethylamine, DMF, 0°C to 25°C, 18 h, 65%.

The target compounds **71** and **72** were synthesized in accordance with **Scheme 11**, wherein 4-(pyridin-2-ylcarbamoyl)benzoic acid was heated with thionyl chloride to

form the corresponding acid chloride (**64**) and subsequently treated with malononitrile to obtain **65**. Trimethyl orthoformate was used to methylate **65**, and then it was treated with hydrazine hydrate at room temperature to generate the pyrazole intermediate (**67**). **67** was reacted with tert-butyl 5-((methylsulfonyl)oxy)hexahydrocyclopenta[*c*]pyrrole-2(1H)-carboxylate and cesium carbonate to get **68**, and that was hydrolysed to an amide (**69**) with hydrogen peroxide and potassium carbonate. Deprotection of the tert-butyl carbamate group of **69** with trifluoroacetic acid led to the formation of an amine intermediate (**70**), which was then acylated by acryloyl chloride to prepare the target compound **71**. In parallel, coupling of but-2-ynoic acid with an amine (**70**) produced the target compound **72** (see experimental section 4.1.11. for detailed procedures).

Scheme 11: Synthetic route of 71 and 72 of Series 4



Reagents and conditions: i) Thionyl chloride, 85°C, 4 h, 99%; ii) Malononitrile, N,N-Diisopropylethylamine, THF, 25°C, 16 h, 98%; iii) Trimethyl orthoformate, 75°C, 16 h, 70%; iv) Hydrazine hydrate, EtOH, 25°C, 16 h, 68%; v) Tert-butyl 5-((methylsulfonyl)oxy)hexahydrocyclopenta[c]pyrrole-2(1H)-carboxylate, cesium carbonate, DMF, 90°C, 16 h, 59%; vi) Hydrogen peroxide, Potassium carbonate, EtOH, DMSO, 45°C, 1 h, 65%; vii) Trifluoroacetic acid, DCM, 25°C, 5 h, 88%; viii) Acryloyl chloride, N,N-Diisopropylethylamine, DCM, 0°C to 25°C, 18 h, 52%; ix) but-2-ynoic acid, O-(1H-Benzotriazol-1-yl)-N,N,N',N'-tetramethyluronium hexafluorophosphate, N,N-Diisopropylethylamine, DMF, 0°C to 25°C, 18 h, 58%.

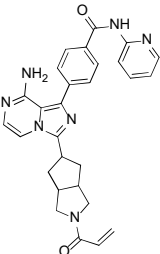
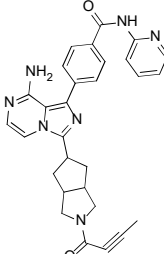
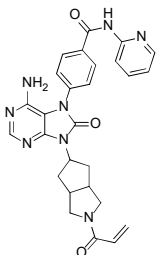
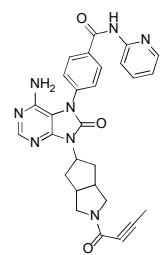
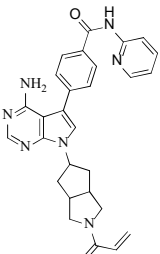
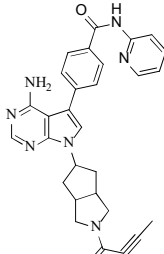
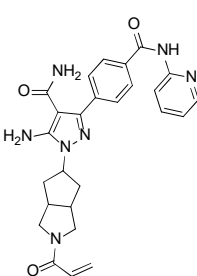
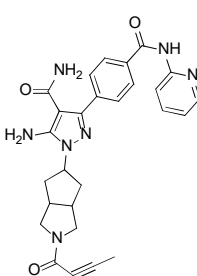
2.5.2. Biological evaluation of Series 4

2.5.2.1. *In vitro* BTK inhibitory and anti-proliferative activity

In the **Series 4**, Pyrrolo-pyrimidine, Oxo-purine, Imidazo-pyrazine, and Pyrazole scaffolds were introduced as hinge binders instead of Pyrazolo-pyrimidine. Total eight molecules (**41**, **42**, **51**, **52**, **61**, **62**, **71**, and **72**) were synthesised and evaluated to determine their *in vitro* BTK enzyme inhibitory and anti-proliferative activity in the **Series 4** (see experimental section 4.2.1., and 4.2.2. for detailed assay protocol). The findings of the *in vitro* assay are summarized in **Table 11**.

The Oxo-purine-based compounds with acrylamide (**51**) and butynamide (**52**) warheads showed moderate inhibitory activities with IC₅₀ values ranging from 12 to 25 nM. Imidazo-pyrazine and Pyrazole-based compounds were found to inhibit BTK enzyme (IC₅₀ = 5.4 nM, 3.6 nM, 4.3 nM, and 5.1 nM of **41**, **42**, **71**, and **72**, respectively) and TMD8 cell proliferation (IC₅₀ = 4.9 nM, 3.0 nM, 1.9 nM, and 3.8 nM of **41**, **42**, **71**, and **72**, respectively) with fairly comparable activities. Only the Pyrrolo-pyrimidine-based hinge binders (**61** and **62**) were found to be nearly as efficacious as the Pyrazolo-pyrimidine-based compounds (**32b** and **32ao**). **61** and **62** exhibited IC₅₀ values of 2.4 nM and 2.9 nM in the BTK enzyme inhibition assay and 2.5 nM and 3.3 nM in the TMD8 cell proliferation assay, respectively.

Table 11. *In vitro* BTK enzyme and TMD8 cell proliferation inhibitory data of 41, 42, 51, 52, 61, 62, 71, and 72 of Series 4

Comp.	Chemical structure	BTK IC ₅₀ (nM) ^a	TMD8 IC ₅₀ (nM) ^b	Comp.	Chemical structure	BTK IC ₅₀ (nM) ^a	TMD8 IC ₅₀ (nM) ^b
41		5.4	4.9	42		3.6	3.0
51		25.1	12.0	52		20.2	16.4
61		2.4	2.5	62		2.9	3.3
71		4.3	1.9	72		5.1	3.8

All the data are shown as the mean for three experiments. ^aBTK inhibition (IC₅₀) determination using *in vitro* BTK kinase assay on ADP Glo platform, ^bTMD8 cytotoxicity inhibition (IC₅₀) determination using TMD8 cell lines assay.

2.5.2.2. CYP and hERG inhibitory activities of the lead compound of Series 4

61 was subjected for CYP and hERG inhibitory studies from **Series 4** as it was found to have the most potent inhibitory activity in BTK enzyme and TMD8 cell proliferation

assays. **61** was incubated with human liver microsomes and NADPH in the presence of CYP-specific substrates to evaluate CYP inhibitory activities (see experimental section 4.2.3. for detailed procedures). The automated patch clamp assay was used to assess hERG inhibitory activities (see experimental section 4.2.7. for detailed procedures). **61** was found to be devoid of hERG at 10 μ M concentration, however, CYP inhibition data indicates that the pyrrolo-pyrimidine analogue (**61**) inhibits CYP isoforms (>50% inhibition of 2C8 and 2D6) at 10 μ M concentration (**Table 12**). As a result, **61** was not explored further for pharmacokinetic studies.

Table 12. CYP and hERG inhibitory activity of the lead compound of Series 4

Comp.	%hERG ^a inhibition @ 10 μ M	% CYP inhibition ^b @ 10 μ M					
		CYP1A2	CYP2C8	CYP2C9	CYP2D6	CYP2C19	CYP3A4
61	28	17	57	43	57	7	11
IBR	35	NI	81	86	31	39	55

^a In the automated patch clamp assay, ^b incubated test compound with human liver microsomes and NADPH in the presence of CYP specific substrate, value are mean of three repeat experiment, NI = No inhibition.

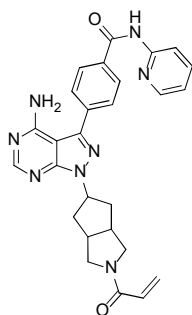
2.6. Developmental studies of **32b**

Several compounds were found to have potent *in vitro* BTK inhibitory and anti-proliferative activity; however, subsequent screening for CYP and hERG liabilities narrowed their number to a few, particularly **24e**, **32b**, and **32ao**. It was discovered that **32b** had a better *in vivo* pharmacokinetic profile than **24e**, **32ao**, and IBR, when the pharmacokinetic profiles of **24e**, **32b**, **32ao**, and IBR (positive control) were evaluated (**Table 4**, **7**, and **10**). Moreover, molecular modelling of **32b** validates that it has potent BTK inhibitory activity related to its covalent binding to the BTK enzyme (see section 2.3.3.). Because of its encouraging preliminary biological features, **32b** was adjudged a potential candidate for developmental studies. Wherein **32b** was assessed for biological efficacy studies, comprising anti-tumor activity in the TMD8 xenograft

model and anti-arthritic efficacy in the collagen-induced arthritis (CIA) mice model. The covalent binding, kinase selectivity, metabolic stability, permeability, and plasma protein binding of **32b** also were determined. Finally, repeat-dose acute toxicity studies (14 days) in rats were carried out to evaluate the safety profile of **32b**. The physicochemical characteristics of **32b** are described in the next sections.

2.6.1. Physicochemical characteristics of **32b**

Structure:



Molecular Formula: $C_{27}H_{26}N_8O_2$

Molecular Weight: 494.56 g/mole

Colour: White coloured powder

Solubility: **32b** was soluble in organic solvents such as DMF, NMP and DMSO and sparingly soluble in dichloromethane (DCM). **32b** demonstrated pH-dependent solubility in aqueous media. The solubility was measured as 500 $\mu\text{mol/L}$ in an acidic pH of 1.2 and decreased to less than 2 $\mu\text{mol/L}$ in purified water and buffers of pH values of 6.8 and 4.5.

Ionization Constant (pKa): 7.2 (calculated)

pH of the compound: 8.75 (1% in water suspension)

Melting Point: 256.3°C

Thermal analysis (DSC): onset at 144.52°C and peak at 145.49°C

Crystallographic Properties: Amorphous (by XRD)

2.6.2. ADME profile of **32b**

2.6.2.1. Caco-2 permeability

32b showed low to moderate permeability across the Caco2 cells monolayer and was found to be a substrate of efflux transporters. The apparent permeability (P_{app}) was 33 nm/sec with an efflux ratio of 5:1 (experimental section 4.2.7. for detailed procedure).

2.6.2.2. Metabolic stability

In mouse, rat, dog, and human liver microsomes, **32b** was discovered to be highly to moderately stable, however it was unstable in monkey liver microsomes. **32b** metabolised only up to 13% in mouse liver microsomes ($mClint$: 0.46 mL/min/g liver), while in rat liver microsomes, 55% of **32b** was metabolised ($mClint$: 2.62 mL/min/g liver). In dog and human liver microsomes, **32b** was metabolised at rates of 18% ($mClint$: 0.67 mL/min/g liver) and 32% ($mClint$: 1.28 mL/min/g liver), respectively. Interestingly, the stability of **32b** was much lower in monkey liver microsomes (66% metabolised with $mClint$ of 3.49 mL/min/g of liver) (see experimental section 4.2.8., for detailed procedure).

2.6.2.3. Plasma protein binding

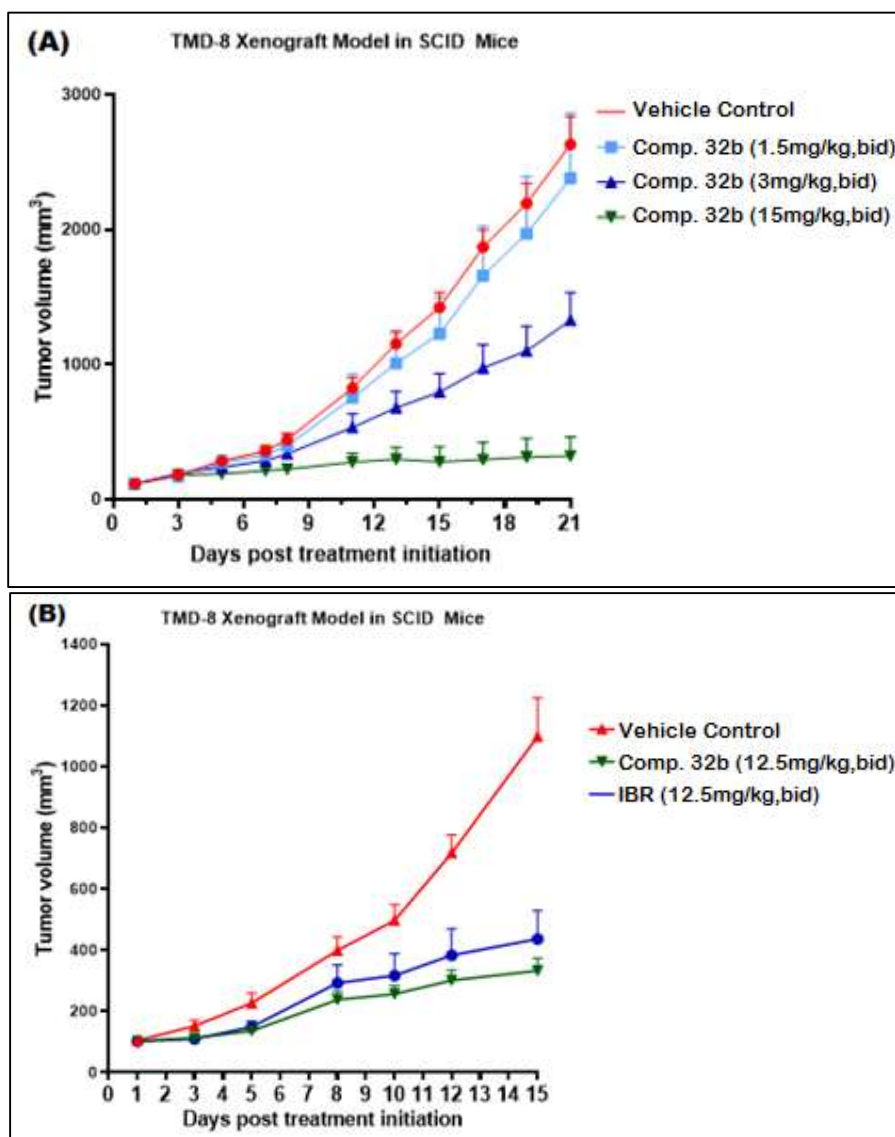
32b showed accepted plasma protein binding ability in rat and human plasma (91.2% and 98.4% in rat and human, respectively) (see experimental section 4.2.9., for detailed procedure).

2.6.3. *In vivo* efficacy studies of **32b**

2.6.3.1. Antitumor activity of **32b** in TMD8 xenograft model

To validate the *in vitro* anti-proliferative effect of **32b** in an *in vivo* system, the anti-tumor potential of **32b** was assessed in TMD-8 DLBCL xenograft tumor-bearing mice (see experimental section 4.2.6.1. for detailed protocol). Animals were treated with 1.5, 3, and 15 mg/kg, BID, of **32b** for 20 days via the oral route of administration. The

tumour volume was measured as described in the experimental section 4.2.6.1. **32b** showed dose-dependent tumour growth inhibition (10%,50%, and 88%, respectively). The growth inhibitory property of **32b** was more prominent after 7 days and onwards (**Figure 18A**). We also compared the efficacy of **32b** (12.5 mg/kg) against IBR (12.5 mg/kg) for its antitumor activities. Our results demonstrated that **32b** had slightly better potency compared to IBR (**Figure 18B**) at the same dose. It is important to note that **32b** does not have any effect on the body weight of the animals during the 20-day treatment period (**Figure 18C**). Thus, the *in vivo* study validates the antitumor potential of **32b**.



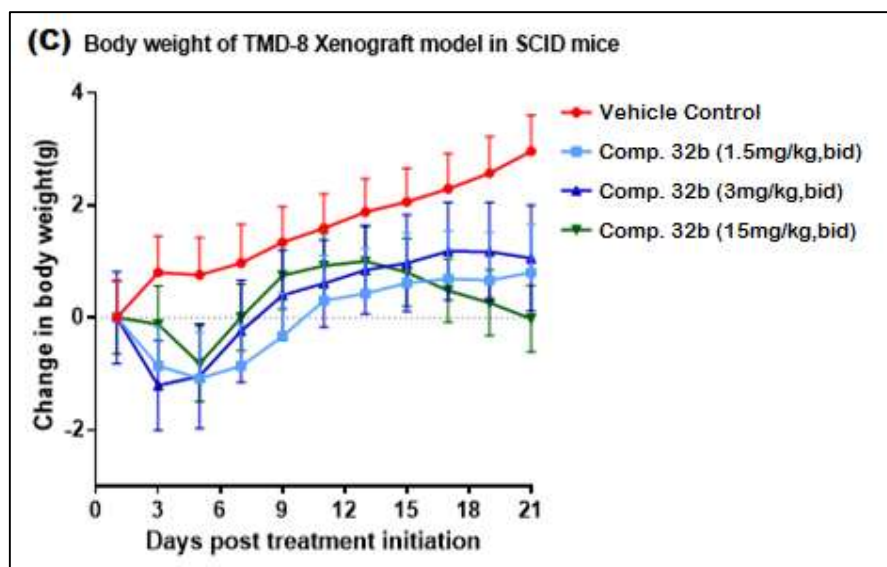


Figure 18. *In vivo* Anti tumor activities of 32b

(A) Suppression of tumor volume in TMD8 DLBCL xenograft model by **32b**. Mice with established tumor reaching around 100 mm³ were divided into different groups of 10 mice each. Groups were untreated vehicle (triangle) or treated with **32b** [1.5 (square), 3 (triangle), and 15 mg/kg (inverted triangle), BID] for 20 consecutive days. The data represents the mean tumor volume. (B) Suppression of tumor volume in TMD8 DLBCL xenograft model by **32b** and IBR. Mice with established tumor reaching around 100 mm³ were divided into different groups of 10 mice each. Groups were untreated vehicle or treated with **32b** or IBR (12.5 mg/kg, BID) for 14 consecutive days. The data represents the mean tumor volume. (C) Effects of **32b** on body weight of mice treated in TMD8 DLBCL xenograft model. Mice with established tumor reaching around 100 mm³ were divided into different groups of 10 mice each. Groups were untreated vehicle or treated with **32b** (1.5, 3 and 15 mg/kg, p.o., BID) for 20 consecutive days. The data represents the mean body weight. Error bars represent SEM. *, P < 0.05 when compared with vehicle control.

2.6.3.2. Anti-arthritis efficacy of 32b in a collagen-induced arthritis (CIA) mice model

Arthritis was developed in male DBA1j mice using a collagen mixture, and mice were recruited for the study once clinical signs were visible. Ten animals were assigned to each of the three groups [vehicle, positive control (IBR, 0.6 mg/kg), and test compound **32b** (0.5 mg/kg)]. Treatment was continued for four weeks, once daily, and the percentage inhibition in the clinical score was recorded (see experimental section 4.2.6.2. for detailed protocol). Also, to check dose-dependent anti-arthritis activity, doses of 0.125, 0.25, 0.5, and 1 mg/kg of **32b** were administered orally, once daily, for

28 days. The study results indicated that **32b** was far more *in vivo* efficacious compare to IBR. **32b** (0.5 mg/kg) caused a 93% reduction in clinical score, while IBR (0.6 mg/kg) showed only a 40% reduction in clinical score in the CIA model. **32b** efficacy was found to be dose related, as the reductions in clinical score were 22 %, 61 %, 93 %, and 97 %, per doses of 0.125, 0.25, 0.5, and 1 mg/kg, respectively (**Figure 19A**).

As shown in **Figure 19A**, treatment with **32b** significantly suppressed the progression of disease; 0.25 mg/kg of **32b** once daily was the lowest dose, which showed improvement in clinical signs of disease after two days of initial dosing. The inflammation and damage to the paw were also assessed histologically. Treatment with **32b** displayed a reduction in the paw swelling based on lower histologic severity scores in the **32b** treated groups compared with the vehicle control. The paws from the vehicle-treated control group had a group mean severity of 10.4, while the mean severity scores in the **32b** treated mice were 5, 3.75, 1, and 0.2 at dosages of 0.125, 0.25, 0.5, and 1 mg/kg, respectively (**Figure 19B**). The body weights of the animals were also recorded three times a week as a measure of treatment-related side effects. No changes in the mice's body weight were observed in any treatment group compared to the vehicle control group (**Figure 19C**). Thus, the improved PK of **32b** justifies its potent *in vivo* efficacy in the CIA mice model.

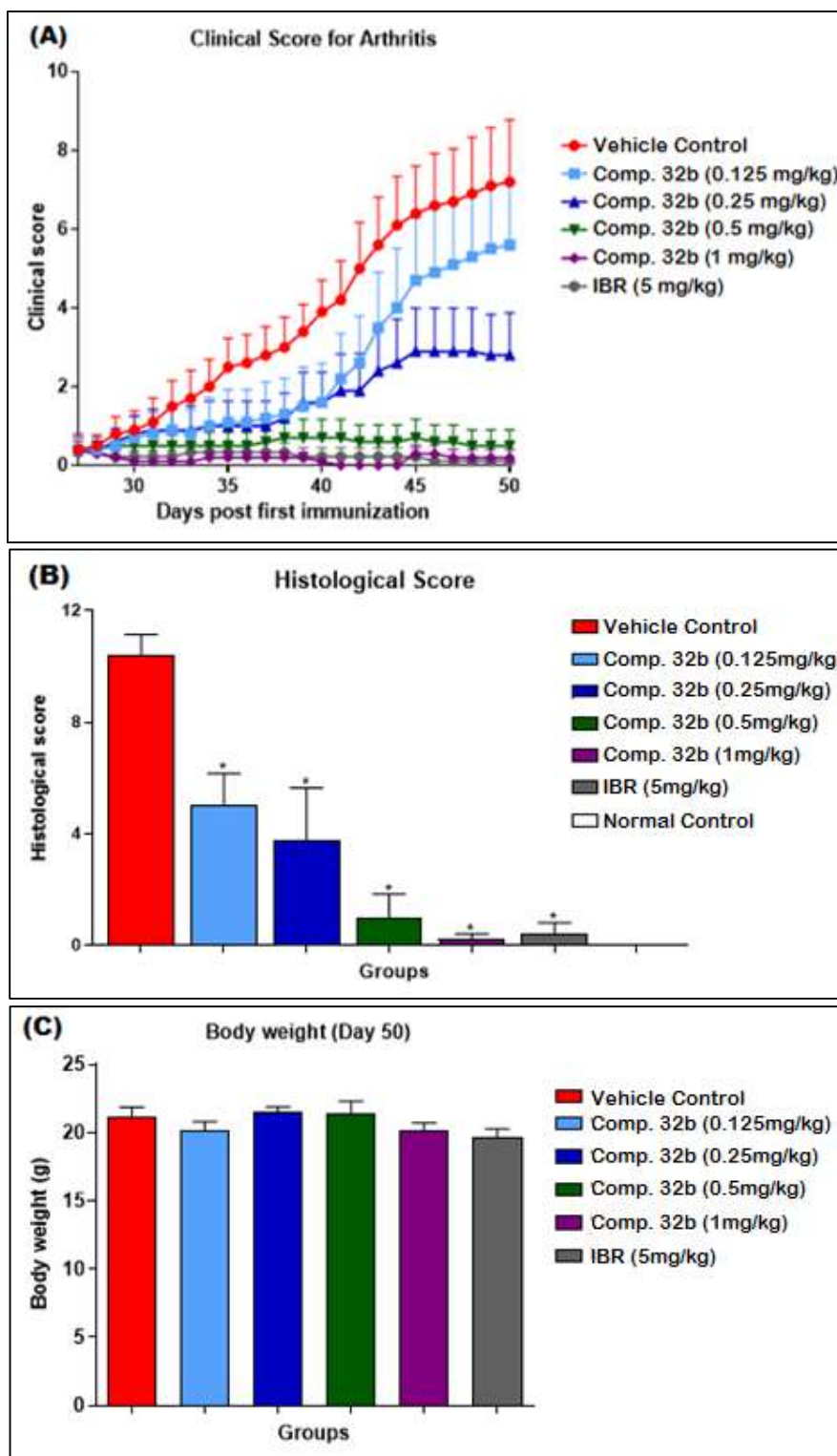


Figure 19. *In vivo* Antiarthritic activities of 32b

(A) Clinical score and (B) Histological score in collagen-induced arthritis (CIA) model. Mice with established CIA were divided into separate groups consisting of 10 mice each. Groups were treated with vehicle (circle) or **32b** [0.125 (square), 0.25 (triangle), 0.5 (inverted triangle), and 1 mg/kg (diamond), QD] for 20 consecutive days. The data represent the mean arthritic or

histological scores. (C) Effect of **32b** on body weight after three weeks of treatment in collagen-induced arthritic mice model. Mice with established CIA were divided into separate groups consisting of 10 mice each. Groups were treated with vehicle or **32b** (0.125, 0.25, 0.5, and 1 mg/kg, OD) for three weeks. The data represents the mean body weight. Error bars represent SEM. *, $P < 0.05$ when compared with vehicle control.

2.6.4. Irreversible (covalent) binding of **32b** to the BTK enzyme

To determine that **32b** was irreversibly bonded to the BTK enzyme, we followed the technique described by Honigberg et al [94]. The first FDA-approved BTK inhibitor, IBR, was shown to be covalently bonded to the BTK enzyme by using the mentioned technique. We used fluorescence-tagged IBR (IBR-BFL) in a THP-1 cell-based binding assay. Analysis of the fluorescent gel showed a fluorescent band at 70 kDa, corresponding to the molecular weight of BTK enzyme. The band started appearing at 0.5 $\mu\text{mol/L}$ IB-BFL and attained saturation at 5 $\mu\text{mol/L}$ and higher concentrations (**Figure 20A**). Immunoblotting of the same gel with anti-BTK Ab confirmed the presence of constant levels of total BTK with increasing concentrations of IB-BFL (**Figure 20A**). This indicated that IB-BFL binds to BTK enzyme, and the binding is detectable at and above 0.5 $\mu\text{mol/L}$. This step was important to find out the concentration of IB-BFL to be used in our corresponding assays. Since 5 $\mu\text{mol/L}$ of IB-BFL was saturating the binding, we chose a sub saturating concentration of 2 $\mu\text{mol/L}$ for the following experiment. In order to test whether IBR and **32b** bind to the same site on BTK enzyme, we adopted a competition binding assay. In this assay, THP-1 cells were pre incubated with an increasing concentration of **32b**, followed by incubation with 2 $\mu\text{mol/L}$ of IBR-BFL. **Figure 20B**, clearly showed that IBR-BFL could either replace or occupy free sites at a **32b** concentration lower than 5 $\mu\text{mol/L}$. However, on increasing the concentration of **32b** to 10 $\mu\text{mol/L}$ and above, the IBR-BFL-BTK interaction was no longer detectable. Since the levels of BTK enzyme did not change (**Figure 20B**), this demonstrated that **32b** binds to the same site as IBR and

that the binding is irreversible in nature. A densitometric scan of the fluorescent bands yielded an IC_{50} of 1 nmol/L for this binding (**Figure 20C**).

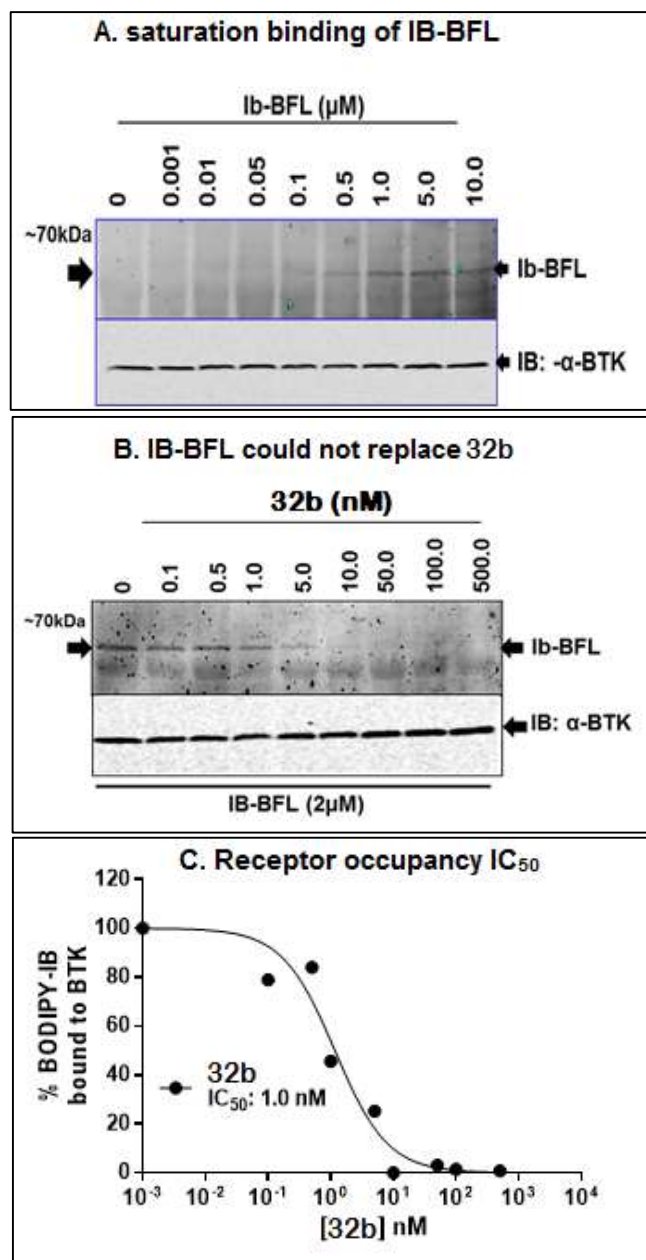


Figure 20. 32b is an irreversible inhibitor of BTK

(A) IBR binds to BTK enzyme and saturation of binding occurs at 5 $\mu mol/L$ and above. (B) IBR failed to replace **32b** from BTK enzyme. (C) **32b** achieved 50 percent receptor (BTK) occupancy at 1 nmol/L. Figures are representative of three independent experiments. **Figure 20C** represents the densitometric scanning data of the same gel as in **Figure 20B** and error bars are not incorporated.

2.6.5. Kinase selectivity of 32b

BTK is among the 11 kinases (TEC, SRC, and EGFR family) having cysteine residues at the structurally equivalent position in the ATP binding domain. For additional profiling studies, **32b** was evaluated for kinase selectivity in a biochemical enzyme inhibition assay, and IC₅₀ values (**Table 13**) were determined. Screening of a panel of 13 different kinases demonstrated that **32b** is highly selective for BTK and TEC, while for other tyrosine kinases, namely ITK, FGR, HCK, and JAK3, **32b** was found to be 350 times less potent. Overall, **32b** was found to be more BTK and TEC selective.

TEC, BTK, ITK, and BMX belong to the non-receptor tyrosine kinase families. Several BTK inhibitors showed potent binding affinity to TEC, which is expressed in CLL cells at similar levels as BTK, suggesting that concomitant binding to both of these kinases could contribute to the anti-tumor effect. On the other hand, binding to both BTK and TEC in platelets is related to bleeding as an adverse effect of BTK inhibitor treatment.

Since **32b** showed similar binding affinity for BMX and TEC, **32b** was subjected to BMX and TEC inhibitory activity in a cellular assay using a BMX and TEC Nano BRET target engagement intracellular kinase assay. In the BMX and TEC Nano BRET kinase assays, **32b** showed less than 10 % inhibition at 1 μ M concentration (EC₅₀ (Tracer 4, BMX / TEC) = >1 μ M), which indicates that the potent binding affinity of **32b** for BMX and TEC in biochemical assays does not translate into cellular assays.

Similar observations were reported earlier for some other BTK inhibitors, wherein biochemical assay data did not correlate with the cellular assay result. For example, in the biochemical assay, Acalabrutinib showed potent TEC inhibitory activity (IC₅₀ = 37 nM). However, in a TEC phosphorylation assay (using human platelets), Acalabrutinib does not inhibit TEC up to a non-pharmacological concentration of less than 1 μ M

(<25% of TEC phosphorylation at 1 μ M concentration). Overall, the *in vitro* selectivity of **32b** against BMX and TEC in cellular assays also justifies that the *in vivo* antiarthritic efficacy and antitumor activity of **32b** are mainly associated with selective BTK inhibition.

Table 13. Biochemical kinase selectivity of 32b

Kinases	IC ₅₀ (μ mol/L) ^a
	32b
BTK	0.027-0.041
ITK	18-24
JAK3	>10
TEC	0.025-0.038
ERBB2 wt	1.7-2.3
EGF-R wt	2.3-3.5
BLK	1.1-2.2
BMX	0.091-0.12
ERBB4	0.12-0.19
EGFRT790M	4.2-5.7
FGR	10-13
FRK	1.3-1.7
HCK	>10

^aIC₅₀ values with range found from three independent experiments.

2.6.6. Safety profile of 32b

Oral doses were administered to groups of five male and female rats. Once day for 14 days, at doses of 50, 100, and 300 mg/kg of compound **32b**. Considering that the ED₅₀ dose was 3 mg/kg as determined by the CIA model studies, these doses are 16x, 33x, and 100x of the ED₅₀, respectively.

To assess the safety profile of **32b**, repeat-dose acute toxicity studies (14 days) were carried out in male Wistar rats, and various parameters such as gross pathology, clinical signs, body weight, organ weight, serum chemistry, and haematological changes were recorded (see experimental section 4.2.10. for detailed protocol). Oral doses were administered to groups of five male and female Wistar rats. Once a day for 14 days, at

doses of 50, 100, and 300 mg/kg of compound **32b**, considering that the ED₅₀ dose was 3 mg/kg as determined by the CIA model, these doses are 16x, 33x, and 100x of the ED₅₀, respectively. Daily oral administration of compound **32b** over a period of 2 weeks did not affect the survival of Wistar rats, and also no adverse changes related to gross pathology, clinical signs, body weight, or feed consumption were noticed, compared to the control group (Table 14). As shown in Tables 15 and 16, the hematological parameters of compound **32b** were found to be comparable to those of control animals. Similarly, compound **32b** showed no significant changes in the serum hepatotoxicity assessment parameters as compared to the control group. Also, the compound **32b** treated groups showed no changes in the key organ weights such as the heart, kidney, spleen, brain, etc. (Table 17).

Table 14. Body weight of rats during treatment of 32b

Duration	Male rats				Female rats			
	Vehicle ^a	32b ^a			Vehicle ^a	32b ^a		
		50	100	300		50	100	300
		mg/kg	mg/kg	mg/kg		mg/kg	mg/kg	mg/kg
Day 1	253±27	261±27	248±23	259±22	172±14	175±10	179±14	177±14
Day 7	273±27	283±30	278±21	278±25	184±17	180±8	187±15	183±12
Day 14	289±29	307±31	301±22	295±29	190±17	187±10	194±14	186±11

^a Values expressed as mean ±SD: *n* = 5, Male and female Wister rats, vehicle = Tween-80 + 0.5% Methyl Cellulose (1:99), administered through Oral gavage route.

Table 15. Hematological parameters after two weeks treatment of 32b

Parameter	Male rats				Female rats			
	Vehicle ^a	32b ^a			Vehicle ^a	32b ^a		
		50 mg/kg	100 mg/kg	300 mg/kg		50 mg/kg	100 mg/kg	300 mg/kg
WBC	6.1	5.9	6.5	6.5	4.5	6.8	7.0	6.2
(10 ³ /μL)	±1.8	±1.7	±1.2	±0.6	±1.2	±1.0	±1.2	±1.3
RBC	8.1	7.9	8.4	8.05	7.0	7.4	7.1	7.3
(10 ⁶ /μL)	±0.4	±0.5	±0.2	±0.5	±0.6	±0.3	±0.6	±0.1
HGB	14.5	15	15.2	14.8	12.7	14.0	13.7	13.7
(g/dL)	±0.6	±0.5	±0.5	±0.5	±1.4	±0.4	±1.4	±0.2
HCT (%)	47.5	49	49.2	47.6	41.8	45.2	43.9	43.8
	±2.0	±1.5	±1.1	±1.5	±4.1	±1.3	±4.1	±0.7
MCHC	30.6	30.8	30.9	31.1	30.3	31.1	31.3	31.2
(g/dL)	±0.1	±0.3	±0.4	±0.3	±0.5	±0.4	±0.5	±0.1
PLT	638	686	721	783	504	861	852	825
(10 ³ /μL)	±64	±110	±98	±58	±168	±92	±76	±81
NEUT	0.76	0.86	1.11	1.11	0.72	0.84	1.07	1.13
(10 ³ /μL)	±0.21	±0.20	±0.34	±0.19	±0.21	±0.13	±0.23	±0.25
LYMPH	4.7	4.5	4.7	4.90	3.3	5.3	5.2	4.45
(10 ³ /μL)	±1.6	±0.35	±0.76	±0.35	±0.85	±1.08	±0.77	±1.13
MONO	0.37	0.30	0.37	0.25	0.31	0.34	0.42	0.33
(10 ³ /μL)	±0.15	±0.11	±0.20	±0.11	±0.12	±0.11	±0.15	±0.11
EOSIN	0.05	0.12	0.13	0.08	0.06	0.19	0.18	0.13
(10 ³ /μL)	±0.02	±0.02	±0.03	±0.02	±0.03	±0.13	±0.05	±0.07
BASO	0.17	0.11	0.18	0.17	0.07	0.15	0.14	0.12
(10 ³ /μL)	±0.07	±0.06	±0.06	±0.06	±0.04	±0.03	±0.02	±0.06

^a Values expressed as mean ±SD; *n* = 5, Male and female Wister rats, vehicle = Tween-80 + 0.5% Methyl Cellulose (1:99), administered through Oral gavage route.

Table 16. Serum chemistry parameter after two weeks treatment of 32b

Parameter	Male rats				Female rats			
	Vehicle ^a	32b ^a			Vehicle ^a	32b ^a		
		50 mg/kg	100 mg/kg	300 mg/kg		50 mg/kg	100 mg/kg	300 mg/kg
GLU	108.16	89.92	81.28	82.46	85.54	92.08	98.60	102.48
(mg/dL)	±19.74	±8.44	±7.13	±9.88	±15.27	±12.57	±5.07	±11.14
TRI	177.08	147.74	180.92	145.22	68.94	57.20	87.80	56.56
(mg/dL)	±58.29	±16.56	±62.40	±39.75	±20.30	±14.04	±44.57	±17.03
TCHOL	69.70	77.74	86.02	77.60	60.80	64.63	60.54	52.88
(mg/dL)	±13.01	±9.50	±14.55	±10.84	±11.65	±12.48	±19.52	±6.97
AST (U/L)	92.62	85.32	72.46	86.18	102.82	72.48	72.94	93.60
	±24.13	±18.31	±9.52	±5.52	±53.82	±4.16	±10.95	±22.63
ALT (U/L)	33.52	38.22	36.90	38.26	42.84	42.30	44.44	40.54
	±6.69	±5.19	±11.96	±6.18	±10.11	±4.83	±8.41	±8.24
ALP (U/L)	106.98	113.92	99.58	110.14	56.76	47.43	46.84	41.02
	±35.57	±33.02	±35.99	±14.51	±8.09	±15.06	±10.12	±9.16
TBIL	0.09	0.09	0.09	0.07	0.10	0.11	0.13	0.10
(mg/dL)	±0.02	±0.01	±0.02	±0.02	±0.02	±0.01	±0.03	±0.01
TP (g/dL)	6.16	6.30	6.52	6.32	6.78	7.15	6.80	6.60
	±0.23	±0.19	±0.26	±0.22	±0.28	±0.19	±0.23	±0.37
ALB	4.46	4.28	4.62	4.40	4.92	5.33	5.18	5.10
(g/dL)	±0.24	±0.19	±0.15	±0.12	±0.22	±0.10	±0.15	±0.33
GLB	1.70	2.02	1.90	1.92	1.86	1.83	1.62	1.50
(g/dL)	±0.10	±0.08	±0.20	±0.13	±0.15	±0.15	±0.16	±0.12
CREAT	0.40	0.41	0.39	0.41	0.55	0.45	0.51	0.49
(mg/dL)	±0.04	±0.05	±0.03	±0.03	±0.04	±0.02	±0.02	±0.05
UREA	33.40	46.60	47.50	42.60	48.78	50.10	49.30	49.60
(mg/dL)	±3.11	±5.60	±8.10	±6.70	±4.46	±7.30	±3.40	±7.30
Ca (mg/dL)	10.66	10.99	11.33	11.06	10.73	11.52	11.35	11.00
	±0.27	±0.16	±0.26	±0.24	±0.27	±0.11	±0.30	±0.19
PHOS	6.40	6.24	6.62	6.50	5.64	5.93	5.92	5.82
(mg/dL)	±0.48	±0.43	±0.34	±0.58	±0.31	±0.67	±0.37	±0.54
Na ⁺	143.80	146.00	146.00	146.00	144.60	146.75	146.40	145.80
(mmol/L)	±0.84	±1.00	±0.00	±1.22	±0.89	±0.96	±1.95	±0.84
K ⁺	4.61	4.13	3.98	4.00	4.70	3.96	3.93	3.97
(mmol/L)	±0.24	±0.28	±0.20	±0.22	±0.12	±0.19	±0.34	±0.27
Cl ⁻	99.88	101.56	100.88	101.14	102.56	103.53	103.34	103.42
(mmol/L)	±1.17	±1.52	±0.72	±0.71	±0.96	±1.18	±0.99	±1.39

^a Values expressed as mean ±SD: *n* = 5, Male and female Wister rats, vehicle = Tween-80 + 0.5% Methyl Cellulose (1:99), administered through Oral gavage route.

Table 17. Relative organ weights (%) after two weeks treatment of 32b

Organ	Male rats				Female rats			
	Vehicle ^a	32b ^a			Vehicle ^a	32b ^a		
		50 mg/kg	100 mg/kg	300 mg/kg		50 mg/kg	100 mg/kg	300 mg/kg
Adrenals	0.048 ±0.008	0.055 ±0.009	0.052 ±0.007	0.055 ±0.011	0.058 ±0.009	0.057 ±0.003	0.057 ±0.005	0.051 ±0.003
Liver	8.579 ±1.664	8.462 ±0.824	8.624 ±0.669	8.769 ±1.635	5.386 ±0.749	5.534 ±0.516	5.453 ±0.591	5.303 ±0.578
Thymus	0.373 ±0.096	0.320 ±0.075	0.368 ±0.046	0.422 ±0.065	0.360 ±0.120	0.346 ±0.098	0.314 ±0.027	0.306 ±0.034
Spleen	0.561 ±0.085	0.535 ±0.050	0.531 ±0.079	0.476 ±0.071	0.365 ±0.048	0.355 ±0.037	0.312 ±0.030	0.271 ±0.028
Heart	0.842 ±0.074	0.984 ±0.184	0.973 ±0.087	0.857 ±0.102	0.607 ±0.023	0.656 ±0.058	0.609 ±0.090	0.607 ±0.075
Kidneys	1.621 ±0.144	1.741 ±0.133	1.807 ±0.120	1.731 ±0.318	1.138 ±0.159	1.254 ±0.109	1.115 ±0.128	1.136 ±0.126
Brain	1.856 ±0.081	1.930 ±0.098	1.822 ±0.039	1.884 ±0.121	1.175 ±0.021	1.753 ±0.039	1.764 ±0.079	1.705 ±0.049
Testes	3.017 ±0.322	3.140 ±0.203	3.010 ±0.554	3.046 ±0.186	-	-	-	-
Epididymis	0.924 ±0.072	1.000 ±0.098	0.926 ±0.104	0.926 ±0.101	-	-	-	-
Ovaries with oviduct	-	-	-	-	0.112 ±0.015	0.094 ±0.016	0.101 ±0.008	0.096 ±0.010
Uterus with cervix	-	-	-	-	0.434 ±0.058	0.413 ±0.161	0.452 ±0.162	0.368 ±0.110

^a Values expressed as mean ±SD: *n* = 5, Male and female Wister rats, vehicle = Tween-80 + 0.5% Methyl Cellulose (1:99), administered through Oral gavage route.